MODIS vegetation products as proxies of photosynthetic potential: A look across meteorological and biologic driven ecosystem productivity

Natalia Restrepo-Coupe[1], Alfredo Huete[1], Kevin Davies[1,7], James Cleverly[2,8], Jason Beringer[3], Derek Eamus[2,8], Eva van Gorsel[4], Lindsay B. Hutley[5], Wayne S Meyer[6]

[1] {Plant Functional Biology and Climate Change Cluster, University of Technology Sydney, PO Box 123, Broadway, NSW, 2007, Australia}

[2] {School of Life Sciences, University of Technology Sydney, PO Box 123, Broadway, NSW, 2007, Australia}

[3] {School of Earth and Environment, The University of Western Australia, Crawley, WA, 6009, Australia}

[4] {CSIRO Oceans and Atmosphere, Forestry House, Building 002, Wilf Crane Crescent, Yarralumla, ACT 2601, Australia}

[5] {Research Institute for the Environment and Livelihoods, Charles Darwin University, Darwin, NT 0909, Australia}

[6] {Environment Institute, School of Biological Sciences, University of Adelaide, Adelaide, SA, 5005, Australia}

[7] {School of Geosciences, University of Sydney NSW 2006, Australia}

[8] {Australian SuperSite Network}

Correspondence to: N. Restrepo-Coupe (nataliacoupe@gmail.com) and A. Huete (alfredo.huete@uts.edu.au)

Type of paper: Primary Research Article

Keywords: OzFlux, Australia, seasonality, ecosystem productivity, cross-site, MODIS, eddy covariance

Abstract

A direct relationship between gross ecosystem productivity (*GEP*) estimated by the eddy covariance (EC) method and Moderate Resolution Imaging Spectroradiometer (MODIS) vegetation indices (VIs) has been observed in many temperate and tropical ecosystems. However, in Australian evergreen forests, and particularly sclerophyll and temperate woodlands, MODIS VIs do not capture seasonality of *GEP*. In this study, we re-evaluate the connection between satellite and flux tower data at four contrasting Australian ecosystems, through comparisons of *GEP* and four measures of photosynthetic potential, derived via parameterization of the light response curve: ecosystem light use efficiency (*LUE*), photosynthetic capacity (*Pc*), *GEP* at saturation (GEP_{sat}), and quantum yield (α), with MODIS vegetation satellite products, including VIs, gross primary productivity (GPP_{MOD}), leaf area index (LAI_{MOD}), and fraction of photosynthetic active radiation ($fPAR_{MOD}$). We found that satellite derived biophysical products constitute a measurement of ecosystem structure (e.g. leaf area index - quantity of leaves) and function (e.g. leaf level photosynthetic assimilation capacity - quality of leaves), rather than *GEP*. Our results show that in primarily meteorological-driven (e.g. photosynthetic active radiation, air temperature and/or precipitation) and relatively aseasonal ecosystems (e.g. evergreen wet sclerophyll forests), there were no statistically significant relationships between *GEP* and satellite derived measures of greenness. In contrast, for phenology-driven ecosystems (e.g. tropical savannas), changes in the vegetation status drove *GEP*, and tower-based measurements of photosynthetic activity were best represented by VIs. We observed the highest correlations between MODIS products and *GEP* in locations where key meteorological variables and vegetation phenology were synchronous (e.g. semi-arid *Acacia* woodlands) and low correlation at locations where they were asynchronous (e.g. Mediterranean ecosystems). Although, we found a statistical significant relationship between the seasonal measures of photosynthetic potential (*Pc* and *LUE*) and VIs, where each ecosystem aligns along a continuum, we emphasize here that knowledge of the conditions in which flux tower measurements and VIs or other remote sens-

ing products converge greatly advances our understanding of the mechanisms driving the carbon cycle (phenology and climate drivers) and provides an ecological basis for interpretation of satellite derived measures of greenness.

1. Introduction

Eddy flux towers constitute a powerful tool to measure and study carbon, energy and water fluxes. Even though the number of eddy covariance (EC) sites has been steadily increasing (Baldocchi, 2014; Baldocchi et al., 2001), instrumentation, personnel costs, and equipment maintenance limit the establishment of new sites. This is demonstrated by the distribution of flux towers around the world and in particular the under-representation of tropical and semi-arid locations in the southern hemisphere (Australia, Africa, and South America) (http://fluxnet.ornl.gov/maps-graphics and Beringer et al. (2007)). The first EC tower was established in 1990 at Harvard Forest (Wofsy et al., 1993) followed by five other sites in 1993 (Baldocchi, 2003). In Australia, only two locations, Howard Springs (AU_How; Hutley et al., 2000) and Tumbarumba (AU_Tum; Leuning et al., 2005), have a record that extends more than 10 years.

Many applications rely on large-scale, remotely sensed (RS) representations of vegetation dynamics (greenness) to: (1) up-scale water and carbon fluxes from the limited tower footprint (radius <10 km) representative of eddy covariance measurements, (2) scale fluxes in time and extend a longer time series from limited tower data, (3) fill gaps due to quality control in the flux measurements, (4) study continental phenology to be validated at flux tower sites, and (5) parameterise land surface and agricultural models to be tested at EC locations. Where satellite derived greenness indices (VIs) represent a community property of chlorophyll content, leaf area index (*LAI)*, and fractional vegetation cover; past studies have focused on the relationship between the Moderate Resolution Imaging Spectroradiometer, (MODIS) VIs, such as the enhanced vegetation index (*EVI*), and tower based measurements of gross ecosystem productivity (*GEP*) (Gamon et al., 2013; Huete et al., 2008, 2006; Maeda et al., 2014; Sims et al., 2006; Wang et al., 2004). A simple linear regression between seasonal (monthly or 16-day) *EVI* and *GEP* has previously provided a good coefficient of determination (R^2) for different ecosystems:

$$GEP = b_0 + b_1 \times EVI \quad (1)$$

where b_0 and b_1 are the fitted coefficients. Huete et al.(2006) reported an R^2 of 0.5 for Eq. 1 in tropical forests and converted pastures over the Amazon basin, and an R^2 of 0.74 in dry to humid tropical forest sites in Southeast Asia (Huete et al., 2008). Over the North Australian mesic and xeric tropical savannas, R^2 ranged from 0.52 at a wooded grassland (Alice Springs, AU-ASM) to 0.89 in woodlands (Howard Springs, AU-How) (Ma et al., 2013).

Similar relationships to Eq. 1 have been explored using monthly maximal net ecosystem exchange (NEE_{max}):

$$NEE_{max} = b_0 + b_1 \times EVI \quad (2)$$

This regression showed an improved fit in forests (R^2=0.83 for deciduous and R^2=0.72 for coniferous forests) compared to the *GEP-EVI* model (R^2=0.81 for deciduous and R^2=0.69 for evergreen forests) (Olofsson et al., 2008).

Other approaches to link carbon fluxes to RS products include radiation-greenness (R-G) models, where both a meteorological driver, represented by the photosynthetic active radiation (*PAR*), and a vegetation phenology driver, represented by *EVI* or by the normalized difference vegetation index (*NDVI*), are implicitly included in the model (Ma et al., 2014; Peng and Gitelson, 2012). By definition, the *GEP*/*PAR* ratio is commonly referred as ecosystem light use efficiency (*LUE*), where:

$$LUE = b_0 + b_1 \times EVI \quad (3)$$

However, the *EVI versus LUE* relationship has shown lower R^2 values (0.76) compared to the *EVI versus GEP* regression (0.92) for a group of North American ecosystems that included evergreen needleleaf and deciduous forests, grasslands and savannas (Sims et al., 2006). Hill et al. (2006) also reported an R^2 of ~0.2 for the *NDVI versus LUE* relationship for the Australian sclerophyll forest of Tumbarumba (AU_Tum), however, the result was not statistically significant ($p>0.05$). To better represent *GEP* at rainfall-driven semi-arid ecosystems, Sjöström et al. (2011) increased the level of complexity of the R-G model by scaling down observations of *PAR* using the evaporative fraction (*EF*) term from EC measurements (a proxy for water availability), thus *GEP* was calculated as:

$$GEP = EVI \times PAR \times EF \qquad (4)$$

where *EF* is the ratio between latent heat flux (*LE*) and the surface turbulent fluxes (*H+LE*), and *H* is defined as the sensible heat flux, $EF = LE/(H+LE)$. The model increased the predictive power of the R-G model in some ecosystems; however, it was not applicable at regional scales due to its reliance upon supporting tower measurements.

Temperature-greenness models (T-G) use the MODIS Land Surface Temperature product (*LST*) and VIs to calculate *GEP* as in Sims et al. (2008). The T-G *GEP* model for nine North American temperate EC sites was calculated as:

$$GEP = EVI_{scaled} \times LST_{scaled} \times m \qquad (5)$$

where *m* is a function of mean annual *LST* and plant functional type (different formulation provided for evergreen and deciduous vegetation), LST_{scaled} is the minimum of two equations (LST / 30) and (2.5 – (0.05 x LST)), and EVI_{scaled} is EVI – 0.10. A similar T-G model, used by Wu et al. (2011), showed high correlation at deciduous forests (R^2= ~0.90) and lower R^2 values at non-forest areas (R^2=0.27 to 0.91) and evergreen forests (R^2=0.28 to 0.91).

Other more complex derivations, including the C-Fix model (Veroustraete et al., 2002) and the MODIS Gross Primary Productivity product (GPP_{MOD}), rely on biome specific relationships that include: (1) vegetation phenology represented by MODIS derived fraction of absorbed *PAR* that a plant canopy absorbs for photosynthesis and growth ($fPAR_{MOD}$); and (2) air temperature (T_{air}), water vapour pressure deficit (*VPD*), and *PAR* as climate drivers (Running et al., 2000). When applied to Australian ecosystems, the GPP_{MOD} (collection 4) was able to estimate the amplitude of the *GEP* annual cycle in an temperate evergreen wet sclerophyll forest (*Eucalyptus* dominated), however, it was out-of-phase (Leuning et al., 2005). For a tropical savanna (AU-How), GPP_{MOD} (collection 5) overestimated dry season *GEP* (Kanniah et al., 2009). Even though, GPP_{MOD} (collection 4.8) at AU-How accurately represented seasonality in productivity; low estimates of *PAR* and other model input variables were compensated by abnormally high $fPAR_{MOD}$ values (Kanniah et al., 2009). A clear indication of obtaining a good result for the wrong reasons.

Besides the difficulties inherent in determining *GEP* in diverse ecosystems, all of the complex models (e.g. GPP_{MOD} and T-G model) require *in situ* measurements of water fluxes, *PAR*, and/or biome classification information to calibrate or derive some variables and consequently, regression coefficients do not necessarily extend to ecosystem types other than those for which the derivation was obtained. In this work, we revisit the *GEP versus EVI,* and *GEP versus* GPP_{MOD} regressions at different sites. Rather than attempting to determine the "best performing model", our first objective was to gain an understanding of ecosystem behaviour. We look at particularly challenging land cover classes: seasonal wet-dry and xeric tropical savannas, Mediterranean environments characterized by hot and dry summers (Mallee), and temperate evergreen sclerophyll forests. The selected locations are part of the OzFlux eddy-covariance network and represent sites where previous studies have shown satellite derived *GEP* models to be unable to replicate *in situ* measurements.

Our second objective was to derive using the light response curve different ground-based measures of vegetation photosynthetic potential: quantum yield (α), photosynthetic capacity (*Pc*), *GEP* at saturation light (GEP_{sat}), and ecosystem light use efficiency (*LUE*) in an attempt to separate the vegetation structure and function (phenology) from the climatic drivers of productivity. We explore d the seasonality of the four measures of photosynthetic potential (α , *Pc, LUE,* GEP_{sat}) and aimed to determine if *EVI* was able to replicate absolute value and their annual cycle rather than photosynthetic activity (*GEP*), based on linear regressions. Similarly, we included in our analysis other MODIS biophysical datasets (*NDVI*, LAI_{MOD}, and $fPAR_{MOD}$) in an effort to understand how to interpret different satellite measures of greenness and how these products can inform modellers and ecologists about vegetation phenology. In contrast to biome-specific classification approaches, we treated the relationship between greenness and photosynthetic potential to be a continuum and therefore, we explored multiple site regressions.

Finally, we combined satellite-derived meteorology (radiation, precipitation and temperature) and biological drivers (vegetation phenology) to determine site specific and multi-biome *GEP* values using multiple regression models. In this study, we evaluated the advantages of introducing both types of variables; we determine if the regressions hold across biomes, and whether productivity processes are driven by phenology, light, water availability and temperature; and we infer which of these variables govern the *GEP* seasonal cycle for each particular ecosystem. These results advance our understanding of driving mechanisms of the carbon cycle (climate, biological adaptation, or a combination of both), temporal and spatial scaling, and provide an ecological basis for the interpretation of satellite derived measures of greenness and phenology products.

2. Methods

2.1. Study sites

The OzFlux infrastructure network is operated by a collaborative research group and was set up to provide the Australian and global ecosystem modelling communities with CO_2 and H_2O flux and meteorological data (Beringer et al., in this issue). We selected four contrasting long-term eddy flux (EC) sites from the OzFlux network (Figure 1 and Table 1) for this study.

In northern Australia the Howard Springs (AU-How) eddy flux tower is located in the Black Jungle Conservation Reserve, an open woodland savanna dominated by an understory of annual grasses and two overstory tree species: *Eucalyptus miniata* and *Eucalyptus tentrodonata* (Hutley et al., 2011; Kanniah et al., 2011). In the middle of the continent, among the xeric tropical savannas, the Alice Springs Mulga site (AU-ASM) is located in a semi-arid Mulga woodland dominated by *Acacia aneura* and different annual and perennial grasses including Mitchell Grass (gen. *Astrebla*) and Spinifex (gen. *Triodia*) (Cleverly et al., 2013; Eamus et al., 2013). Classified as a Mediterranean environment and characterized by hot and dry summers, the Calperum-Chowilla flux tower (AU-Cpr), is located at the fringes of the River Murray floodplains, a Mallee site (multi-stemmed *Eucalyptus socialis* and *E. dumosa* open woodland) (Meyer et al., 2015). The evergreen Tumbarumba (AU-Tum) site is located in Bago State Forest, NSW and classified as temperate evergreen wet sclerophyll (hard-indigestible leaves) forest. It is dominated by 40 m tall *Eucalyptus delegatensis* trees (Leuning et al., 2005; van Niel et al., 2012).

Fluxes at all towers were measured by the EC method with an open-path system. Simultaneously, an array of different sensors measured meteorological data including air temperature (T_{air}), relative humidity (RH), incoming and reflected short wave radiation (SW_{down} and SW_{up}), and incoming and reflected long wave radiation (LW_{down} and LW_{up}). Refer to each site references for complete information regarding ecosystem and measurement techniques.

2.2. Eddy covariance data

We used Level 3 OzFlux data that includes an initial OzFlux standard quality control (QA) (Isaac et al., in this issue). All data were subject to the same quality assurance procedures and calculations, providing methodological consistency among sites and reducing the uncertainty of the calculated fluxes. We performed additional quality checks and removal of outliers, and data were corrected for low turbulence periods (see Section 2.2.1). Ecosystem respiration (R_{eco}) and *GEP* were calculated from EC measurements of net ecosystem exchange (*NEE*) as presented in Section 2.2.2. Finally, we derived different measures of ecosystem vegetation photosynthetic potential (Section 2.2.3).

2.2.1. Eddy covariance and meteorological measurements

Incoming and outgoing radiation, both shortwave (SW_{down}, and SW_{up}) and longwave (LW_{down} and LW_{up}), were measured using a CNR1 Net Radiometer instrument (Campbell Scientific). All sensors were placed above the canopy at the same height or higher than the EC system. As there were no measurements of *PAR* radiation available at AU-ASM, AU-Tum and AU-Cpr, we assumed $PAR = 2 x SW$ (Papaioannou et al., 1993; Szeicz, 1974), where *PAR* is measured as flux of photons (μmol m^{-2} s^{-1}) and SW_{down} as heat flux density (W m^{-2}). We understood this as an approximation because *PAR* radiation (0.4 -0.7 nm) is a spectral subset of SW_{down} (0.3 – 3 nm).

At AU-Tum, the *NEE* is calculated as the sum of the turbulent flux measured by eddy covariance (F_C) plus changes in the amount of CO_2 in the canopy air space (storage flux, S_{co2}), where $NEE= F_C + S_{co2}$.

At all other sites, given the sparse vegetation cover and the smaller control volume over the vegetation which is lower in height, F_C is assumed to be representative of *NEE*.

Hourly fluxes measured during rainy periods, when the sonic anemometer and the open path infrared gas analyser (IRGA) do not function correctly, were identified and removed from the time series. We also removed isolated observations (between missing values). We identified any residual spikes from the hourly *NEE* data using the method proposed by Papale et al. (2006) and modified by Barr et al. (2009). For each hour (*i*), the measure of change in *NEE* (d_i) from the previous (i-1) and next (i+1) time step is calculated as:

$$d_i = (NEE_i - NEE_{i-1}) - (NEE_{i+1} - NEE_i) \quad (6)$$

A spike is identified if the change is outside a given range:

$$Md - \left(\frac{z * median|d_i - Md|}{0.6745}\right) < d_i > Md + \left(\frac{z * median|d_i - Md|}{0.6745}\right) \quad (7)$$

where *Md* is the median of the differences (d_i), ±0.6745 are the quartiles for a standard normal distribution, and the constant *z* was conservatively set to 5 (Restrepo-Coupe et al., 2013).

2.2.2. Ecosystem respiration (R_{eco}) and gross ecosystem productivity (*GEP*)

Night-time hourly *NEE* values were corrected for periods of low turbulent mixing by removing them from the time series data. Low turbulent missing periods were determined when friction velocity ($u*$ in m s-1) was below a threshold value ($u*_{thresh}$) as described in Restrepo-Coupe et al. (2013). Table 1 presents site-specific $u*_{thresh}$ values and the corresponding upper and lower confidence bounds.

Night-time *NEE* is assumed to be representative of ecosystem respiration (R_{eco}) and it is calculated by fitting R_{eco} to a second-order Fourier regression based on the day of the year (*DOY*) as in Richardson and Hollinger (2005):

$$R_{eco} = fo + s_1 \sin(Dpi) + c_1 \cos(Dpi) + s_2 \sin(2\,Dpi) + c_2 \cos(2\,Dpi) + e \tag{8}$$

where, f_o, e, s_1, c_1, s_2, and c_2 are the fitted coefficients and $Dpi = DOY\ x\ 360/365$ in radians. This method calculates R_{eco} with minimal use of environmental covariates. In order to determine the consistency of the Fourier regression method and the low friction velocity (u*) filter on the modelled R_{eco} (directly dependent of night-time *NEE* values), we compared the results presented here to R_{eco} values based on the intercept of the relation (rectangular hyperbola) between *NEE* and SW_{down} (for no incoming radiation, $SW_{down} = 0$) (Suyker and Verma, 2001) (Supplement Figure 1).

Gross ecosystem exchange (*GEE*) was calculated as the difference between *NEE* and R_{eco} ($GEE=NEE+R_{eco}$). We defined gross ecosystem productivity (*GEP)* as negative *GEE* (positive values of *GEP* flux indicate carbon uptake). For a 16-day moving window, we fitted two rectangular hyperbolas on the relationship between incoming *PAR* and *GEP* observations (separating morning and afternoon values) as in Johnson and Goody (2011) and based on the Michaelis and Menten formulation (1913):

$$GEP = \frac{\alpha\ x\ GEP_{sat}\ x\ PAR}{GEP_{sat} + (\alpha\ x\ PAR)} \tag{9}$$

where α is the ecosystem apparent quantum yield for CO_2 uptake (the initial slope), and GEP_{sat} is *GEP* at saturating light (the asymptote of the regression) (Falge et al., 2001) (Figure 2). Our intention was to compare 16-day MODIS data to observations rather than to model a complete time series. We therefore, filled infrequent *GEP* missing values only if in a 16 day period there were 30 hours of measurements.

We obtained similar seasonal patterns and good agreement using different methods for calculating *GEP* and R_{eco} (Supplement Fig. 1). We observed no statistically significant seasonal differences between calculating R_{eco} as the intercept of the light response curve (Falge et al., 2001) and *NEE* not subject to $u*_{thresh}$ correction ($R_{eco\ LRC}$), to calculating R_{eco} using the Fourier regression method (slope ~0.87 and R^2=0.94 linear regression between $R_{eco\ LRC}$ and R_{eco}). This comparison increased our confidence in using either method to derive *GEP* and R_{eco} fluxes from the EC data, the absolute values and the seasonality here presented.

GEP and *GPP* (true photosynthesis minus photorespiration (Wohlfahrt and Gu, 2015)) have been used interchangeably in the literature. However, *GPP* in this study was distinguished from *GEP*, thus as *GEP* does not include CO_2 recycling at leaf-level (i.e. re-assimilation of dark respiration) or below the plane of the EC system (i.e. within canopy volume) (Stoy et al., 2006). This differences may be important when comparing tower-flux observations of *GEP* to the MODIS *GPP* (see next section).

2.2.3. Four measures of ecosystem photosynthetic potential: *α*, *LUE*, GEP_{sat}, and *Pc*

Measures of photosynthetic potential constitute an attempt to separate the inherent vegetation properties that contribute to photosynthetic activity (*GEP*) from the effects of the meteorological influences on productivity using the paramatrization of the 16-day light response equation. The variables *α*, *LUE*, GEP_{sat}, and *Pc* were intended to represent an ecosystem property, a descriptor of the vegetation phenology similar to leaf area index (*LAI*) or above ground biomass (*AGB*). We calculated 16-day mean α and GEP_{sat}, which are the two coefficients that define the *GEP versus PAR* rectangular hyperbola (Eq. 5) as a measure of the vegetation structure and function (Figure 2). Both α (μmol CO_2 $mmol^{-1}$) and GEP_{sat} (μmol CO_2 m^{-2} s^{-1}) values are known to vary with vegetation type, temperature, water availability and CO_2 concentration. GEP_{sat} represents the ecosystem response at saturating levels of *PAR*, usually constrained by high vapour pressure deficit (*VPD*), air temperature (T_{air}), water availability, and foliar N, among other variables (Collatz et al., 1991; Ehleringer et al., 1997; Tezara et al., 1999). By contrast, α is measured at low light levels, when diffuse radiation is high (cloudy periods, sunset and sunrise). Ecosystem light use efficiency (*LUE*) was defined as the mean daily *GEP/PAR* ratio. Therefore, *LUE* includes the effect of day length, the radiation environment (diffuse *versus* direct), water availability and other physical factors.

We used the relationships between tower measured *GEP*, *PAR*, and *VPD* to characterize the photosynthetic capacity of the ecosystem (*Pc*). Where *Pc* was defined as the average *GEP* for incoming radiation at light levels that are non-saturating -values between the annual daytime mean *PAR* ± 100 μmol m^{-2} s^{-1} (940, 1045, 788 and 843 μmol m^{-2} s^{-1} at AU-How, AU-ASM, AU-Tum and AU-Cpr, respectively) and *VPD* ranges between annual daytime mean ±2 standard deviations (Figure 2) (Hutyra et al., 2007; Restrepo-Coupe et al., 2013). *Pc* was interpreted as a measure of the built capacity without taking into account the day-to-day changes in available light, photoperiod, and extreme *VPD* and *PAR* values. The derivation of *Pc* did not take into account other variables such as T_{air} or soil water content.

2.3. Remote sensing data

2.3.1. Moderate Resolution Imaging Spectroradiometer (MODIS)

We retrieved MODIS reflectances, VIs and other products from the USGS repository covering the four eddy flux locations. Data were subject to quality assurance (QA) filtering, and pixels sampled during cloudy conditions and pixels adjacent to cloudy pixels were rejected (for a complete list of QA rules see Supplement Table 1). Other QA datasets and/or fields related to the above products that were not included on the original metadata were not examined as part of the quality filtering process.

At each site we extracted either a 1 km window (or a 1.25 km window depending on MODIS product resolution – see Table 2) centred on the location of the flux tower. The mean and standard deviation of all pixels were assumed to be representative of the ecosystem. The derivative data collection included the following MODIS data (also see Table 2):

MCD43A1: The 8-day 500m (Collection 5) Nadir Bidirectional Reflectance Distribution Function (BRDF) Adjusted Reflectance (NBAR) product was used to derive the enhanced vegetation index (EVI_{SZA30}) and the normalized vegetation index ($NDVI_{SZA30}$) at fixed solar zenith angle of 30° (available for 2003 to 2013):

$$NDVI_{SZA30} = \frac{NIR_{SZA30} - R_{SZA30}}{NIR_{SZA30} + R_{SZA30}} \quad (10)$$

$$EVI_{SZA30} = \frac{G\,x\,(NIR_{SZA30} - R_{SZA30})}{NIR_{SZA30} + (C1\,x\,R_{SZA30}) - (C2\,x - B_{SZA30}) + L} \quad (11)$$

where R_{SZA30}, NIR_{SZA30} and B_{SZA30} are the red, near infrared, and blue band BRDF corrected reflectances, and coefficients G=2.5, C1=6, C2 = 7.5, and L=1 (Huete et al., 1994). Both VIs are measures of greenness and have been designed to monitor vegetation, in particular photosynthetic potential and phenology (Huete et al., 1994; Running et al., 1994). However, the *EVI* has been optimized to minimize the effects of soil background, and to reduce the impact of residual atmospheric effects.

We labelled the NBAR VIs as EVI_{SZA30} and $NDVI_{SZA30}$ to differentiate them from the MOD13 VI product (*EVI and NDVI*), and emphasize the values here presented include a BRDF correction that is aimed to remove the influence of sun-sensor geometry on the reflectance signal (Schaaf et al., 2002).

MOD15A2: The Leaf Area Index (LAI_{MOD}), and Fraction of Photosynthetically Active Radiation ($fPAR_{MOD}$) absorbed by vegetation from atmospherically corrected surface reflectance products (Knyazikhin et al., 1999). Data were filtered to remove outliers present in the $fPAR_{MOD}$ and LAI_{MOD} time series using Eq. 3. A threshold value of 6 for the *z* coefficient was calibrated to remove 8-day variations of ±50% on $fPAR_{MOD}$, and ±3-4 units in LAI_{MOD}.

MOD17A2: The 8-day Gross Primary Production (GPP_{MOD}) and Net Photosynthesis (*PsnNet*) (collection 5.1). The GPP_{MOD} is calculated using the formulation proposed by Running et al. (2000) and relies on satellite derived short-wave downward solar radiation (SW_{down}), $fPAR_{MOD}$, maximum light-use-efficiency (ε_{max}) obtained from a biome-properties look-up table, and maximum daily *VPD* (VPD_{max}) and minimum daily air temperature (T_{min}) from forcing meteorology:

$$GPP_{MOD}=\varepsilon max \times 0.45 \times SW_{down} \times fPAR_{MOD} \times f(VPD_{max}) \times f(T_{min}) \quad (12)$$

where only the highest quality data were selected for the analysis.

MOD11A2: Daytime Land Surface Temperature (LST_{day}) 8-day time-series was included in the analysis in order to study the effect of T_{air}, another important ecosystem carbon flux driver. Thus, as *LST* or skin temperature (temperature at the interface between the surface and the atmosphere) has been proven to be highly correlated to T_{air} (Shen and Leptoukh, 2011).

2.3.2. Satellite measures of precipitation (TRMM) and incoming solar radiation (CERES)

This study incorporated monthly 0.25 degree resolution precipitation data (1998-2013) in units of mm month^{-1} from the Tropical Rainfall Measuring Mission (TRMM) data product (3B43-v7) derived by combining TRMM satellite data, GOES-PI satellite data, and a global network of gauge data (Huffman et al., 2007). We used 1.0° resolution monthly surface shortwave flux down (all-sky) in W m^{-2} from the Clouds and the Earth's Radiant Energy System (CERES) experiment (Gesch et al., 1999). The CERES Energy Balanced And Filled top of the atmosphere (EBAF) Surface_Ed2.8 product provided fluxes at surface, consistent with top of the atmosphere fluxes (CERES- EBAF TOA) (Kato et al., 2012). No quality control was performed on the rain ($Precip_{TRMM}$) or short wave (SW_{CERES}) satellite derived time series. We used satellite derived meteorological variables instead of in situ measurements as the independent variable in GEP models (see Section 2.5), thus, our findings (e.g. regressions) can be extrapolated to regional and continental scales.

2.4. Mean values

All analyses were done on 16-day data, therefore, 8-day MODIS products were resampled to the match the selected temporal resolution. We interpolated lower frequency satellite remote sensing time series (e.g. CERES and TRMM), using a linear regression from the original dataset to 16-days, where the original value corresponds to the centre of the month defined as day 15, and the newly interpolated value will be representative of the middle of the 16-day period.

Mean fluxes and variables from the eddy covariance are reported on a 30 min or hourly basis. Daily averages were calculated if at least 45 out of 48, or 21 out of 24 data points were available for the day. Bi-weekly values were calculated if at least 4 out of the 16 days were available. For analysis and presentation purposes, we averaged all existing 16-day values of EC and RS data to produce a single year, seasonal cycle.

2.5. Evaluation of synchronicity between remote sensing and flux-tower data

We fitted Type II (orthogonal) linear regressions that account for uncertainty in both variables (satellite and EC). We obtained an array of very simple models of productivity and photosynthetic potential. For example, GEP_{RS}, where $GEP_{RS} = b_0 + b_1 \, x$ RS, b_0 and b_1 were site-specific coefficients, and RS are satellite derived products (*EVI*, *fPAR*, etc.). We compared the different models to the observations (*GEP versus* GEP_{EVI}, *GEP versus* GEP_{NDVI}, etc.) using Taylor single diagrams (Taylor, 2001), where the radial distances from the origin are the normalized standard deviation, and the azimuthal position is the correlation coefficient between the GEP_{RS} and *GEP* or any other measure of ecosystem photosynthetic potential (Supplement Fig. 2).

We determined at each site which combination of carbon flux and MODIS index showed good agreement based on statistical descriptors: coefficient of determination, p-value, root-mean-square-error (RMSE), standard deviation (SD) of the observation and model, and the Akaike's Information Criterion (AIC). Thus, we analysed site-specific and cross-site multiple regression models to compare different biological (greenness) and environmental controls (precipitation, temperature, radiation) on productivity. In each ecosystem, *GEP* was modelled as a linear regression using a single independent variable, two-variables, and bivariate models that included an interaction term. For example: (1) $GEP = b_0 + b_1 \, x \, EVI_{SZA30}$, (2) $GEP = b_0 + b_1 \, x \, EVI_{SZA30} + b_2 \, x \, SW_{CERES}$, and (3) $GEP = b_0 + b_1 \, x \, EVI_{SZA30} + b_2 \, x \, SW_{CERES} + b_3 \, x \, EVI_{SZA30} \, x \, SW_{CERES}$, where b_0, b_1, b_2, and b_3 are fitted coefficients by a non-linear mixed-effects estimation method. Additional models derived from the all-site regressions were compared to the site-specific results. We inferred ecosystem adaptation responses to climate (e.g. light harvest adaptation, water limitation, among other phenological responses) from the bivariate models. This analysis is useful for the interpretation of satellite derived phenology metrics and understanding the biophysical significance of different measures of greenness when incorporated into ESM as representative of vegetation status.

3. Results

3.1. Seasonality of *in situ* measurements

In this section we describe the seasonality of *in situ* meteorological measurements to better understand ecosystem carbon fluxes, and to contextualize the differences in vegetation responses to climate. In particular, we contrast seasonal patterns of air temperature (T_{air}), precipitation, and *VPD* across sites, and compare observations of the annual cycle of photosynthetic activity (productivity) and potential (biophysical drivers of productivity) for each ecosystem.

With the exception of AU-How, all sites showed strong seasonality in T_{air} (Fig. 3). However, the timing of mean daily T_{air} minimum and maximum, and the amplitude of the annual values, varied according to site. The smallest range in T_{air} (5°C) occurred at the northern tropical savanna (AU-How), and the largest amplitude (15°C) occurred at the southern temperate locations (AU-Cpr and AU-Tum). The annual cycle of *VPD* followed T_{air} at all locations except AU-How where summer and autumn rains (February-March) lead to a decrease in *VPD* (Figure 3). Precipitation at AU-How was higher and more seasonal than at any other site with a mean monthly rainfall of 152 mm (1824 mm year^{-1}) and ranging from 1 to 396 mm month^{-1}. Incoming radiation at the tropical savanna site (AU-How) did not show clear seasonality (Figure 3). In this tropical savanna (latitude 12.49˚S) the summer solstice, where top of the atmosphere (*TOA*) radiation is highest, coincides with monsoonal cloudiness resulting in reduced surface radiation. By contrast, at temperate sites like AU-Cpr and AU-Tum, the difference in mean daily *PAR* between summer and winter was ~460 μmol m^{-2} s^{-1}. Rainfall was aseasonal at AU-Tum (~78 mm month^{-1}) and was very low at the semi-arid sites of AU-Cpr and AU-ASM with mean precipitation values of 34 and 37 mm month^{-1} respectively.

Productivity in the four ecosystems ranged from a high at AU-How and AU-Tum (Figure 4) (peak 16-day multi-year average *GEP* of 8.4 and 7.7 gC m^{-2} d^{-1} respectively) to a low at AU-Cpr and AU-ASM (peak 16-day annual average *GEP* average of 2.4 and 3.4 gC m^{-2} d^{-1} respectively) (Figure 4). There was a clear seasonal cycle in photosynthetic activity with maxima in the summer at AU-How and AU-

Tum (November-March) and in the autumn (March-April) at AU-ASM and AU-Cpr. The peaks were broader at AU-Tum than at AU-How and at AU-ASM (Figure 4). An additional short-lived increase in *GEP* was apparent at AU-ASM in the spring (October) before the summer wet period (Figure 4a). Supplement Figures 3 and 4 show the diel cycles of *VPD*, *GEP* and other meteorological and flux variables in example summer (January) and winter months (July).

Vegetation phenology, as indicated by the seasonal cycle of photosynthetic potential (*Pc, LUE*, *α*, and GEP_{sat}), diverged from photosynthetic activity (*GEP*) at the southern locations of AU-Tum and AU-Cpr as shown by the differences in the timing of maximum and minimum *GEP* compared to vegetation phenology (Figure 4 and Supplement Fig. 5). At the tropical savanna site (AU-How), ecosystem quantum yield (α) increased gradually in the spring (September), reaching a maximum during the summer month of January in synchrony with *GEP*. In the sclerophyll forest (AU-Tum), α remained at a constant value of ~1.4 gC MJ^{-1} until the middle of the autumn (April-May) when it reached a value of 1.76 gC MJ^{-1}. Maximum GEP_{sat} occurred during the summer at this site (~36 gC m^{-2} d^{-1}) and gradually decreased by the start of the autumn with a winter minimum (20 gC m^{-2} d^{-1}). At AU-Tum, the GEP_{sat} and α were out-of-phase (Figure 4) and although seasonality was limited in GEP_{sat} and α, neither of them matched seasonal fluctuations in *VPD* (cf. Figures 3 and 4). Similar to GEP_{sat}, *LUE* decreased during the summer months and experiences a winter maximum opposite to the annual cycle of *GEP*. Given the high degree of seasonality of *GEP* at AU-Tum, it is interesting that the photosynthetic potential was comparatively less seasonal and asynchronous to productivity. Supplement Fig. 5 shows the relationships between the different measures of ecosystem performance indicating that they are not always linear.

3.2. Seasonality of satellite products

In the tropical savanna (AU-How) the annual cycles of RS products synchronously reached an early summer maximum in January, and high values extended throughout the autumn (Figure 4d and e). By contrast at AU-Cpr, both $NDVI_{SZA30}$ and EVI_{SZA30} peaked in autumn-winter, coinciding with the lowest *GEP* values (Figure 4p and s). EVI_{SZA30} and $NDVI_{SZA30}$ at AU-ASM captured the autumn peak in *GEP* with a maximum in March, however, a spring VI minimum (November) was not observable in *GEP*. At the two semi-arid sites (AU-ASM and AU-Cpr), $fPAR_{MOD}$ was relatively aseasonal, and the amplitude of the annual cycle was ~0.09, with a 0.25-0.34 range at AU-Cpr and lower values between 0.17-

0.26 at AU-ASM (Figure 4o). LAI_{MOD} at AU-Cpr reached a maximum of 0.50 during the autumn (March) and a spring minimum (September) of 0.39. At AU-ASM, the LAI_{MOD} product ranged from 0.17 (December) to 0.27 (April) (Figure 4t). Most RS products (e.g. EVI_{SZA30} and LAI_{MOD}) showed no clear seasonality at AU-Tum (Figure 5i and j).

$fPAR_{MOD}$ *versus* $NDVI_{SZA30}$ were highly correlated at all sites (R^2>0.7, p<0.01) with the exception of the sclerophyll forest (AU-Tum) where $NDVI_{SZA30}$ remained constant in the 0.68 - 0.83 range (R^2=0.01) (Supplement Fig. 6). At the sclerophyll forest site (AU-Tum), the $NDVI_{SZA30}$ reached values close to saturation. Similar to $fPAR_{MOD}$ *versus* $NDVI_{SZA30}$, EVI_{SZA30} *versus* $NDVI_{SZA30}$ was highly correlated (R^2=0.96, all-site regression). However, the timing of minimum and maximum between $NDVI_{SZA30}$ and EVI_{SZA30} differed at AU-Cpr and AU-How (Figure 4 and Figure 5d and s).

3.3. Relationship between MODIS *EVI* and *GPP* and *in situ* measures of ecosystem photosynthetic activity (*GEP*)

In this study we used a simple linear model to predict *GEP* from EVI_{SZA30} and $GPP_{MOD.}$ We observed three patterns. First, in the tropical savanna site (AU-How) there was a highly significant correlation between photosynthetic activity and EVI_{SZA30}, where EVI_{SZA30} explained 82% of *GEP* (Figure 5a). Similarly at AU-ASM, productivity was statistically related to EVI_{SZA30} (R^2= 0.86, p<0.01). However, GPP_{MOD} only explained 49% of *GEP* at AU-How and 48% at AU-ASM (Figure 5e and g).

A second pattern was observed in the sclerophyll forest site (AU-Tum), where the relationship between *GEP* and EVI_{SZA30} was not statistically significant (R^2<0.01 and p=0.93, Figure 5b). At AU-Tum there was a clear seasonal cycle in *GEP* (low in winter and high during the summer) that was not captured by the small amplitude of the satellite derived data (Figure 3). Of the four ecosystems examined, AU-Tum was the only site where GPP_{MOD} showed an improvement (higher predictive value of *GEP*) compared to $EVI_{SZA30.}$ However, as reported in previous works (Leuning et al., 2005), the GPP_{MOD} product was unable to capture the seasonality of the sclerophyll forest as it underestimated the observed summer peak in *GEP* which corresponded to a second minimum in GPP_{MOD}.

Finally, at the semi-arid site (AU-Cpr), we observed R^2 values significantly different from 0 but small R^2 0.34 and 0.24 ($p<0.01$) for *GEP versus* EVI_{SZA30} and *GEP versus* GPP_{MOD}, respectively. This, demonstrated the low predictive power of both satellite products to determine seasonal *GEP* values at this particular Mediterranean ecosystem. In particular the GEP_{EVI} and GPP_{MOD} models tended to under-estimate productivity at low levels (Figure 5d and h).

The relationship between productivity and EVI_{SZA30} was complex across the different Australian ecosystems (Figure 5). The semi-arid site of AU-Cpr and the sclerophyll forest of AU-Tum are particularly interesting because of the inability of EVI_{SZA30} to seasonally replicate *GEP* (Figure 5). An additional analysis that considers the amplitude and phase of the annual cycle (based on all available 16-day observations) was conducted using Taylor plots (Supplement Fig. 7). This analysis showed that EVI_{SZA30} was in-phase and able to predict the range of productivity values at AU-How and AU-ASM, while at the AU-Cpr site the EVI_{SZA30} captured the amplitude of seasonal *GEP*, however, the linear model was out-of-phase. At AU-Tum, the EVI_{SZA30}-based model consistently preceded *in situ* observations (asynchronous) and exaggerated *GEP* seasonality (ratio between the standard deviation of the model and observations was 4.98).

3.4. Relationship between EVI_{SZA30} and measures of photosynthetic potential (α, *LUE*, GEP_{sat}, and *Pc*)

In this section we reconsider our understanding of EVI_{SZA30} by relating it to different measures of photosynthetic potential (α, *LUE*, GEP_{sat}, and *Pc*) across the four sites (Figure 6). Similar to section 3.3, we used a very simple linear model in which EVI_{SZA30} was expected to predict α, *LUE*, GEP_{sat}, and *Pc*. In the regression models for photosynthetic potential the R^2 values were similar to the *GEP* models for AU-How and AU-ASM (cf. Figure 6c and g). However, EVI_{SZA30} *versus* α at AU-How R^2 was relatively low ($R^2<0.4$, $p<0.01$). At the AU-Cpr site, the EVI_{SZA30}-based model was able to improve the timing and amplitude of the annual cycle when used to calculate *LUE*, *Pc* and GEP_{sat} instead of *GEP* (Figure 6 and Supplement Fig. 7).

At the sclerophyll forest site (AU-Tum) the EVI_{SZA30} was able to predict vegetation phenology rather than productivity. For example we observed that *Pc* (but not α) was significantly related to EVI_{SZA30}

(R^2= 0.16, p<0.01; Figure 6 and Supplement Table 4). Even though, the regressions between *LUE*, GEP_{sat}, and *Pc* against EVI_{SZA30} showed higher correlation (R^2~0.13, p<0.01) than the *GEP versus* EVI_{SZA30} relationship (R^2=0.04, p=0.25) at AU-Tum, R^2 values were still low. However, the low R^2 can be explained by the small dynamic range of both seasonal measures of photosynthetic potential and EVI_{SZA30} (cf. Figure 4 and Figure 6).

3.5. Satellite products compared to flux tower based measures of ecosystem potential

In this section we explore other MODIS products (LAI_{MOD}, $fPAR_{MOD}$, and $NDVI_{SZA30}$) to determine if the predictive power of EVI_{SZA30} as a measure of photosynthetic potential (e.g. *Pc*) can be generalised across other satellite-derived biophysical parameters. We aimed to determine for each location, which of the MODIS products capture the seasonality and phenology of vegetation, thereby gaining some insight into the significance of the different VIs and other satellite derived ecosystem drivers. At AU-How and AU-ASM the MODIS LAI_{MOD}, $fPAR_{MOD}$ and VIs showed a larger or similar correlations to *LUE* and *Pc* in comparison to *GEP* (Supplement Table 4, Figure 7a and b and Figure 7i and j, respectively). At AU-How, AU-ASM, and AU-Cpr, based on our analysis using Taylor plots, most RS products were in-phase with the various measures phenology (R^2>0.8 and low RMSE) (Figure 7 and Supplement Figure 2 and Table 4). However, there was a tendency for most RS indices to underestimate the seasonality of the *LUE* annual cycle at all sites (i.e., standard deviation was smaller for LUE_{RS} than the observed, Figure 7). With exception to AU-Tum, all products were able to capture seasonal changes in *Pc* (Figure 6 and Figure 7).

Similar to EVI_{SZA30}, most of the MODIS indices, and in particular $fPAR_{MOD}$ and LAI_{MOD}, showed strong linear relationships with *LUE* and *Pc* at the Mediterranean ecosystem AU-Cpr, where the introduction of phenology represented an important improvement over the RS-derived models (Figure 6 and Figure 7). Similarly, comparable to EVI_{SZA30}, other MODIS products were unable to replicate *GEP* at AU-Tum (Figure 7). However, the small amplitude of seasonality in *LUE* and *Pc* were well characterized by LUE_{RS} and Pc_{RS}, including a winter maximum similar to that in *LUE* (Figure 4), despite underestimating the annual seasonal cycle in the sclerophyll forest (Figure 4 and 7e-h).

3.6. Multi-biome derived linear relationships between VIs and photosynthetic potential (phenology) and activity (productivity)

Our objective was to investigate if one relation fits all flux sites, and which RS products and equations would enable us to extend our analysis from these four key Australian ecosystems to a continental scale. The all-site relationship for MODIS EVI_{SZA30}, $NDVI_{SZA30}$, LAI_{MOD}, and $fPAR_{MOD}$ products (in that order) show the best agreement (phase and amplitude) to seasonality of *LUE* and *Pc* (Figure 7). Correlations increased for relationships built using data for all the ecosystems instead of the site-specific equations with the exception of the AU-ASM site (Figure 7, Figure 8 and Table 3).

Improvements in how satellite products can model biological drivers (photosynthetic potential) instead of productivity *per se*, are clearly seen at the evergreen temperate forest of AU-Tum. At AU-Tum the relationship between *GEP* and any of the satellite products was not statistically significant ($R^2 < 0.1$) with the exception of LST_{day} (Figure 5 and Figure 7). However, skin temperature (LST_{day}) is a meteorological driver or constraint rather than a direct measure of productivity, and the low all-site LST_{day} *versus GEP* correlation was an indication of this ($R^2=0.66$, $p=0.03$; Figure 8).

The wet sclerophyll forest introduced the greatest uncertainties to the linear models across all sites (Figure 8). For example, regressions involving EVI_{SZA30} were exponential, therefore, significantly increasing *GEP* and *LUE* translated into slightly higher EVI_{SZA30} values, a behaviour mostly driven by the observations at AU-Tum. In particular, the relationship between *LUE versus* $fPAR_{MOD}$ and *LUE versus* $NDVI_{SZA30}$ at AU-Tum were problematic as $fPAR_{MOD}$ and $NDVI_{SZA30}$, appeared to "saturate" at 0.9 and 0.8, respectively (Figure 8).

EVI_{SZA30} explained 81% of *Pc* seasonality based on an all-site regression (Supplement Table 4). Similarly, $NDVI_{SZA30}$ showed a high coefficient of determination (0.70 for GEP_{NDVI}, 0.75 for LUE_{NDVI}, and 0.79 for Pc_{NDVI}) (Supplement Table4). The null hypothesis of no correlation was rejected ($p<0.01$) for all regressions between MODIS VIs, LAI_{MOD} and $fPAR_{MOD}$ *versus* photosynthetic potential (phenology) and activity (productivity) (Supplement Table 4). However, statistical significance of *GEP* versus GEP_{RS}, was driven by the AU-ASM and AU-How ecosystems.

Multiple linear regression models used to predict *GEP* by combining satellite derived meteorology and biologic parameters (Table 3) showed large correlations when both drivers were introduced (meteorology and vegetation phenology), with the exception of the AU-Tum site where SW_{CERES} and LST_{day} explained 60% and 58% of *GEP*, respectively, and the AU-ASM and AU-How sites where EVI_{SZA30} and $NDVI_{SZA30}$ explained ~84% and ~80% of the variations in *GEP*, respectively. In particular, at the AU-How site, no significant improvement to the *GEP* model was obtained when combining MODIS VIs with any meteorological variable (R^2 remain similarly high R^2~0.82). By contrast, at the AU-ASM site, EVI_{SZA30}, satellite derived incoming short wave (SW_{CERES}), and the interaction of both significantly increased model correlation with an R^2 of 0.88 and a lower AIC (Akaike's Information Criterion as a measure of model quality) when compared to models relying only on EVI_{SZA30} (R^2=0.85, AIC=64) or SW_{CERES} (R^2=0.02, AIC =209) (Table 3). Similar results were obtained for those regressions driven by EVI_{SZA30} and precipitation at this rainfall pulse driven site (R^2=0.88, AIC=42). At the AU-Cpr site, temperature-greenness models were highly correlated to *GEP* (R^2>0.64), however, the best results (higher R^2 and lower AIC) were obtained for radiation-greenness models, explaining 71% (EVI_{SZA30} - SW_{CERES} and $NDVI_{SZA30}$- SW_{CERES}) of *GEP*. For a complete version of Table 3 that includes all available variable combinations, see Supplement Table 3.

4. Discussion

4.1. Derivation of measures of photosynthetic potential at tropical savannas, sclerophyll forests and semi-arid ecosystems

In this study we were able to separate the biological (vegetation phenological signal) from the climatic drivers of productivity using eddy-covariance carbon exchange data. Using the parametrization of the light response curve we derived different measures of vegetation photosynthetic potential (α, *LUE*, GEP_{sat} and *Pc*). At seasonal time scales (e.g. 16-days, monthly), our analysis looks at the biotic drivers of productivity; whereas at shorter time scales (e.g. hourly, daily) photosynthetic potential can be limited or enhanced by meteorological controls, thus as linked to resource scarcity (i.e. high *VPD* or water constraints), availability (e.g. increase radiation or access to soil water). and the correspondent ecosystem responses (e.g. stomatal closure, CO_2 fertilization) that will determine *GEP*. The variables α, *LUE*, GEP_{sat}, and *Pc* have different biophysical meanings; therefore, we were able to establish physiological explanations for describing why and which RS products and environmental variables relate to them at each ecosystem. For example, GEP_{sat} measured at high levels of *PAR* is prone to be influenced by various environmental factors (*VPD*, T_{air} and soil water availability) and therefore may be a good indicator of canopy stress.

As observed at AU-How, GEP_{sat} was highly and negatively correlated to periods of low precipitation and negatively correlated with *VPD* (Supplement Table 4). Seasonal values of GEP_{sat} at the semi-arid sites (AU-Cpr and AU-ASM) did not show a direct relationship with *VPD* or precipitation. This does not mean that there is no effect of atmospheric demand or soil moisture content on carbon fluxes at shorter time scales (hourly or daily). Compared to GEP_{sat}, we expected α to be less dependent of *VPD* and better reflect vegetation phenology, as α represents the canopy photosynthetic response at low levels of *PAR* characteristic of cloud cover (diffuse light) during early morning or late afternoon periods (Kanniah et al., 2012, 2013). However, among all measures of phenology, α showed one of the lowest site-specific correlations when compared to any of the RS products presented on this study. Our results show that *LUE* and *Pc* showed the best correlations to VIs. Confirmation that this research deals less with the instantaneous responses (GEP_{sat} and α) and rather focuses on the mid-term, 16-day seasonal descriptors of vegetation phenology (*Pc* and *LUE*).

The influence of other environmental factors apart from *PAR* and *VPD*, such as soil water content and T_{air}, is difficult to isolate from the derivation of vegetation descriptors (e.g. specific leaf area, plant chlorophyll and water content) and is probably inherent to ecosystem responses and adaptation to climate, resource competition, and herbivory, among other factors. Moreover, to what degree it is feasible to untangle the relations between climate and vegetation is complex and not well understood, as the feedback processes are essential in ecosystem function (leaf flush, wood allocation, among other vegetation strategies respond to available resources). Our results show that VIs were highly related to *Pc*, which is interpreted as a phenology descriptor that does not consider the day-to-day changes in available light or photoperiod or the vegetation response to high and low *VPD* and *PAR* values. By contrast, implicit in the derivation of *LUE* were the day length and anomalous climatic conditions. This finding has important implications when using EC data for the validation of satellite derived phenology.

4.2. Seasonality and comparisons between satellite products and flux tower based measurements of carbon flux: photosynthetic activity (productivity) and potential (phenology)

Previous satellite derived models of productivity usually apply to locations where the seasonality of *GEP* is synchronous with climatic and vegetation phenology drivers (Mahadevan et al., 2008; Sims et al., 2008; Wu et al., 2010; Xiao et al., 2004), such as in temperate deciduous forests, where temperature and incoming radiation coincide with changes in ecosystem structure and function (e.g. autumn sub-zero temperatures may initiate leaf abscission (Vitasse et al., 2014)). In our analysis, productivity was synchronous with all measures of photosynthetic potential only at the savanna site (AU-How), where clouds and heavy rainfall in the summer wet season resulted in low *VPD*, reduced *TOA* (aseasonal *PAR)*, and minimal fluctuations in T_{air}. At AU-How, we observed a consistently large correlation between MODIS VIs and productivity and no improvement in *GEP* when accounting for meteorology. Moreover, the highly significant EVI_{SZA30} *versus GEP* relationship at AU-How could be generalised to other satellite derived biophysical products.

Arid and semi-arid vegetation dominate ~75% of the Australian continent, and at these ecosystems a characteristic mix of grasses (understory) and woody plants (overstory) contribute to total annual *GEP* at different times of the year. More importantly, the phenology of grasses and trees are driven by, or respond differently to, various climatic drivers (e.g. trees greening up after spring rainfalls while grasses remain dormant (Cleverly et al., 2016; Ma et al., 2013; Shi et al., 2014)). The changing seasonal contributions to the reflectance signal and to *GEP* are generally related to soil water content thresholds. Our study presents two semi-arid *Acacia* and *Eucalyptus* woodlands where we found that models relating VIs with photosynthetic potential (phenology), rather than activity (productivity), improved the predictive power of RS greenness indices (AU-Cpr) or showed similar statistical descriptors (AU-ASM). At the woodland *Acacia* site, LAI_{MOD} and $fPAR_{MOD}$ overestimated the periods of low capacity (associated with browndown phases) (Ma et al., 2013). This can be better understood if we account for small but non-negligible photosynthetic activity in *Acacia* after the summer rains have ended (Cleverly et al., 2013; Eamus et al., 2013). At this particular site (AU-ASM), the high LAI_{MOD} and VIs observed during dormancy may not be interpreted as high photosynthetic potential. Satellite data, and even some ground-based measurements of LAI_{MOD}, cannot differentiate between the different fractional components: photosynthetic active vegetation (*fPAV*), and non-photosynthetic vegetation (*fNPV*). Future work requires phenocams or biomass studies in which *fPV* and *fNPV* may be spectrally or mechanically separated.

In low productivity ecosystems (AU-ASM and AU-Cpr), satellite and EC data/noise ratio may have a considerable effect on the site-specific regressions (e.g. sun geometry influence on VIs seasonal values, and EC uncertainties). However, differences between AU-ASM and AU-Cpr regressions (e.g. EVI_{SZA30} is highly correlated to *GEP* only at AU-ASM) and the fact that the VI product has been corrected for BRDF effects, increases our confidence on the analysis presented here. Moreover, the lower VIs *versus GEP* correlation values obtained at AU-Cpr compared to AU-ASM could be attributed to Mallee site productivity being more dependent on meteorological drivers than photosynthetic potential, or *GEP* being driven by climate (e.g. autumn precipitation –when *Pc* remains constant) or vegetation phenology (e.g. summer *LAI* and canopy chlorophyll content, among others) at different times of the year.

Similar to Mediterranean ecosystems (AU-Cpr), in wet sclerophyll forests (AU-Tum) without signs of water limitation, the VIs were unable to replicate seasonality in *GEP*. In particular, the dominant species of sclerophyll forests, *Eucalyptus*, *Acacias* and *Banksias*, show very little seasonal variation in canopy structure as seen in aseasonal *LAI* observations (Zolfaghar, 2013), and leaf longevity (Eamus et al., 2006). Leaf quantity (e.g. *LAI*) and quality (e.g. leaf level photosynthetic assimilation capacity) are two key parameters in driving photosynthetic potential; when these are aseasonal, asynchronous or lagged, they may confound the interpretation of seasonal measures of greening. Thus, the observed increasing predictive power of VIs as a measure of photosynthetic potential (e.g. EVI_{SAZ30} *versus Pc*, R^2=0.16 at AU-Tum) may not be comparable to similar relationships at sites where vegetation phenology showed a larger dynamic range (e.g. EVI_{SZA30} *versus Pc*, R^2=0.79 at AU-How).

4.3. Considerations for the selection of RS data to be used on *GEP* models and phenology validation studies

This study reports high correlations for *Pc versus* EVI_{SZA30} (R^2=0.81) and *Pc versus* $NDVI_{SZA30}$ (R^2=0.80). The fact that a brighter soil background results in lower *NDVI* values than with a dark soil background for the same quantity of partial vegetation cover (Huete, 1988; Huete and Tucker, 1991) may have a positive effect in the all-site *Pc versus* $NDVI_{SZA30}$ regressions (increase R^2). Thus as darkened soils following precipitation generally result in higher *NDVI* values for incomplete canopies

(Gao et al., 2000) and may similarly suggest higher vegetation or soil biological crust activity. On the other hand, soil brightness and moisture may have a negative effect on the confidence interval of the x-intercept for the proposed relationships (e.g. *Pc* versus $NDVI_{SZA30}$, for $NDVI_{SZA30}$~*0*). Moreover, at certain times the AU-ASM and AU-Cpr sites were at the low end of the vegetation activity range, and the observed RS signal may have been dominated by soil water content rather than by photosynthetic potential. However, caution is needed when using $fPAR_{MOD}$ and other products as we observed a threshold value above which *in situ* changes were undetectable (e.g. MODIS *fPAR*>0.9, $NDVI_{SZA30}$>0.8). This might have been due to the *NDVI* saturating at high biomass (Huete et al., 2002; Santin-Janin et al., 2009).

Temperature-greenness models of *GEP* (Sims et al., 2008; Xiao et al., 2004) take into account the meteorological and biophysical drivers that determine productivity. Nevertheless, correlations between photosynthetic characteristics and LST_{day} were weaker than for VIs. Moreover, if the seasonality of *GEP* is driven by local climatology, as in the case of AU-Tum where *GEP* was statistically correlated to LST_{day}, our intent is to understand the relation between vegetation characteristics and RS products rather than indiscriminately use any satellite-derived index to describe phenology or photosynthetic potential. Our study demonstrates that multiple linear regression models that combine satellite derived meteorology and biological parameters to describe *GEP* fit better when both drivers are introduced rather than when only one factor drives the relation (a single meteorology or greenness variable). However, two exceptions to this rule were observed: (1) at AU-Tum where SW_{CERES} was able to explain 60% of *GEP*, and (2) in the tropical savanna at AU-How where EVI_{SZA30} was able to explain ~82% of the variation in *GEP*, and where we did not obtain any significant improvement to the *GEP* model when combining MODIS VIs and any meteorological variable (R^2 remain similarly high R^2>0.82). In summary, at evergreen sclerophyll forests, even when *GEP* is highly seasonal, *GEP* is driven by meteorology as seen by the fact that most of the measures of photosynthetic potential showed small seasonal changes, similar to different MODIS products. By contrast, sites where most of the *GEP* seasonality was driven by vegetation status (*Pc* as a proxy) rather than the meteorological inputs (*PAR*, air temperature and precipitation), or where meteorology and phenology were synchronous, VIs were strongly correlated to both *GEP* and *Pc* (e.g. tropical savanna). This was in agreement with the expectation than RS products constitute a measurement of ecosystem photosynthetic potential rather than productivity *per se*.

In summary, our analysis shows how MODIS greenness indices were able to estimate different measures of ecosystem photosynthetic potential across biomes. At only one site (AU-Tum) was there very little seasonal variation in EVI_{SZA30}, compared to other evergreen ecosystems. Both the strong correlations among VIs and *Pc* from *in situ* eddy covariance carbon flux measurements at the remaining sites and the positioning of each ecosystem along a continuum of MODIS-derived variables representing vegetation phenology confirms the usefulness of satellite products as representative of vegetation structure and function. This research confirms the viability of satellite-derived phenology to be validated and more importantly, understood, using eddy-flux measurements of *Pc*. However, an increase in effort in determining seasonal patterns of carbon allocation (partition between leaves and wood), understory and overstory responses, and leaf carbon assimilation and chlorophyll content over time, may be required to obtain a more meaningful understanding of RS indices and their biophysical significance. Moreover, the reader should be aware that rapid changes in vegetation phenology (e.g. α and GEP_{sat}) caused by short-term environmental stresses (e.g., temperature, humidity, soil water deficit or waterlogging) may not be accurately estimated by RS products and require the employment of *in situ* high frequency optical measurements (e.g. phenocams), or land surface vegetation models, or direct eddy covariance measurements.

For this study we included all available 16-day data corresponding individually to more than 10 years at AU-How and AU-Tum, and two to three years at AU-Cpr and AU-ASM. The long-term sampling implies that we were likely to be capturing a large range in mean ecosystem behaviour. RS products may over- or under-represent the canopy response to periods of extreme temperature and precipitation, although the time series in this study included warmer than normal years and heat waves, e.g. 2012-2013 (BOM, 2012, 2013; Van Gorsel, in this issue) and wetter than normal years, e.g. 2011 (Fasullo et al., 2013; Poulter et al., 2014) that lead to larger than normal *GEP* at AU-ASM and AU-Cpr (Cleverly et al., 2013; Eamus et al., 2013; Koerber et al., in this issue). It is beyond the scope of this work to evaluate the inter-annual variability of the vegetation responses to disturbance (e.g. insect infestation or fire) or extreme climatic events (e.g. flooding or long term drought). Improvements to satellite derived phenology can be related to an increasing number of EC sites and samples thereby emphasizing the importance of long-term time measurements and sampling of diverse ecosystems.

5. Conclusions

Remote sensing vegetation products have been widely used to scale carbon fluxes from eddy covariance (EC) towers to regions and continents. However, at some key Australian ecosystems MODIS GPP and VIs may not track seasonality of gross ecosystem productivity (*GEP*). In particular, we found EVI_{SZA30} was unable to represent *GEP* at the temperate evergreen sclerophyll forest of Tumbarumba (AU-Tum) and at the Mediterranean ecosystem (Mallee) of Calperum-Chowilla (AU-Cpr). This result extends across satellite products overall: MODIS GPP_{MOD}, LAI_{MOD}, $fPAR_{MOD}$, and other VIs.

We aimed for a greater understanding of the mechanistic controls on seasonal *GEP* and proposed the parametrization of the light response curve from EC fluxes, as a novel tool to obtain ground-based seasonal estimates of ecosystem photosynthetic potential (light use efficiency (*LUE*), photosynthetic capacity (*Pc*), *GEP* at saturation (GEP_{sat}), and quantum yield (α)). And by photosynthetic potential we refer to the presence of photosynthetic infrastructure in the form of ecosystem structure (e.g. leaf area index-quantity of leaves) and function (e.g. leaf level photosynthetic assimilation capacity - quality of leaves) independent of the meteorological and environmental conditions that drive *GEP*. Based on basic linear regressions, we demonstrated that MODIS derived biophysical products (e.g. VIs) were a proxy for ecosystem photosynthetic potential rather than *GEP*. We reported statistically significant regressions between VIs (e.g. $NDVI_{SZA30}$ and EVI_{SZA30}) to long term measures of phenology (e.g. *LUE* and *Pc*), in contrast to ecosystem descriptors subject to short term responses to environmental conditions (e.g. GEP_{sat} and α). Our results should extend to other methods and measures of greenness, including VIs and chromatic coordinates from phenocams and in situ spectrometers.

We found that the linear regressions between MODIS biophysical products and photosynthetic potential converged on a single function across very diverse biome types, which implies that these relationships persist over very large areas, thus improving our ability to extrapolate in situ phenology and seasonality to continental scales, across longer temporal scales and to identify rapid changes due to extreme events or spatial variations at ecotones. We further found that saturation of $fPAR_{MOD}$ and $NDVI_{SZA30}$, restricted their usefulness, except in comparatively low biomass ecosystems (savannas and arid and semi-arid savannas and woodlands).

We quantified how much of *GEP* seasonality could be explained by different variables: radiation (SW_{down}), temperature (T_{air}), precipitation (*Precip*), or phenology (*VIs* as proxy). Our analysis showed the relationship between RS products and *GEP* was only clear when productivity was driven by either: (1) ecosystem phenology and climate, synchronously driving *GEP*, as was observed at Alice Springs Mulga woodland (AU-ASM), and similar to many temperate deciduous locations, or (2) solely by the vegetation photosynthetic potential, as observed at the tropical savanna site of Howard Springs (AU-How). At AU-How, radiation and temperature were constant across the year, although ecosystem photosynthetic activity (*GEP*) and potential (e.g. *Pc* and *LUE*) fluctuated with the highly seasonal understory. However, RS products do not follow *GEP* when: (3) phenology is asynchronous with key meteorological drivers such that *GEP* is driven by one or the other at different times of the year, as we observed at AU-Cpr; or when (4) *GEP* is driven by meteorology (SW_{down}, T_{air}, soil water availability, *VPD*, or different combinations) and photosynthetic potential is aseasonal, as observed at AU-Tum. At AU-Tum, changes in productivity were driven by $\mathrm{SW}_{\mathrm{down}}$,, while the ecosystem biophysical properties remained relatively constant across the year, represented by the small amplitude of the annual cycles in *Pc* and *LUE* (true evergreen forest). An understanding of why satellite versus flux tower estimates of *GEP* relationships hold, or do not hold, greatly contribute to our comprehension of carbon cycle mechanisms and scaling factors at play (e.g. climate and phenology, among others).

Acknowledgements

This work was supported by an Australian Research Council Discovery Research Grant (ARC DP110105479) “Integrating remote sensing, landscape flux measurements, and phenology to understand the impacts of climate change on Australian landscapes and the Australian Government’s Terrestrial Ecosystems Research Network”. TERN (www.tern.gov.au) is a research infrastructure facility established under the National Collaborative Research Infrastructure Strategy and Education Infrastructure Fund (Super Science Initiative) through the Department of Industry, Innovation, Science, Research and Tertiary Education. We utilized data collected by grants funded by the Australian Research Council (DP0344744, DP0772981 and DP130101566). J. Beringer is funded under an Australian Research Council Future Fellowship (ARC FT110100602).

The authors would like to thank our collaborators Professor Scott R. Saleska, Dr. Sabina Belli, and Dr. Piyachat Ratana. Special acknowledgement to Tim Lubcke, Rolf Faux, and Dr. Nicole Grant for technical support at different OzFlux sites.

We show our respect and acknowledge the people, the traditional custodians of the Land, of Elders past and present of the Arrernte Nation at Alice Springs, the Wiradjuri people at Tumbarumba, the Meru people at Calperum-Chowilla and the Woolna nation at Howard Springs.

References

Baldocchi, D.: Measuring fluxes of trace gases and energy between ecosystems and the atmosphere – the state and future of the eddy covariance method, Glob Change Biol, 20(12), 3600–3609, doi:10.1111/gcb.12649, 2014.

Baldocchi, D., Falge, E., Gu, L., Olson, R., Hollinger, D., Running, S., Anthoni, P., Bernhofer, C., Davis, K., Evans, R., Fuentes, J., Goldstein, A., Katul, G., Law, B., Lee, X., Malhi, Y., Meyers, T., Munger, W., Oechel, W., Paw, K. T., Pilegaard, K., Schmid, H. P., Valentini, R., Verma, S., Vesala, T., Wilson, K. and Wofsy, S.: FLUXNET: A New Tool to Study the Temporal and Spatial Variability of Ecosystem–Scale Carbon Dioxide, Water Vapor, and Energy Flux Densities, Bulletin of the American Meteorological Society, 82(11), 2415–2434, doi:10.1175/1520-0477(2001)082<2415:FANTTS>2.3.CO;2, 2001.

Baldocchi, D. D.: Assessing the eddy covariance technique for evaluating carbon dioxide exchange rates of ecosystems: past, present and future, Global Change Biology, 9(4), 479–492, doi:10.1046/j.1365-2486.2003.00629.x, 2003.

Barr, A., Hollinger, D., and Richardson, A. D., 2009, CO2 Flux Measurement Uncertainty Estimates for NACP, AGU Fall Meeting, December 2009, abstract number B54A-04B

Beringer, J., Cleverly, J., Eamus, D., Van Gorsel, E., Hutley, L. B., Meyer, W. S. and Macfarlane, C.: An introduction to the Australian flux tower network - OzFlux, Biogeosciences, in this issue.

Beringer, J., Hutley, L. B., Tapper, N. J. and Cernusak, L. A.: Savanna fires and their impact on net ecosystem productivity in North Australia, Global Change Biology, 13(5), 990–1004, doi:10.1111/j.1365-2486.2007.01334.x, 2007.

BOM: Special Climate Statement 41 - Extreme November heat in eastern Australia, Australian Bureau of Meteorology, Melbourne, Australia., 2012.

BOM: Special Climate Statement 45 - a prolonged autumn heatwave for southeast Australia, Australian Bureau of Meteorology, Melbourne, Australia., 2013.

CERES: Clouds and the Earth’s Radiant Energy System Information and Data, NASA, Langley Research Center, Hampton, VA, USA, available at: http://ceres.larc.nasa.gov/ (last access: 28 August 2015), 2014a.

Cleverly, J., Eamus, D., Van Gorsel, E., Chen, C., Rumman, R., Luo, Q., Restrepo Coupe, N., Li, L., Kliun, N., Faux, R., Yu, Q. and Huete, A.: Productivity and evapotranspiration of two contrasting semiarid ecosystems following the 2011 carbon land sink anomaly, Agricultural and Forest Meteorology, submitted.

Cleverly, J., Boulain, N., Villalobos-Vega, R., Grant, N., Faux, R., Wood, C., Cook, P. G., Yu, Q., Leigh, A. and Eamus, D.: Dynamics of component carbon fluxes in a semi-arid Acacia woodland, central Australia, J. Geophys. Res. Biogeosci., 118(3), 1168–1185, doi:10.1002/jgrg.20101, 2013.

Collatz, G. J., Ball, J. T., Grivet, C. and Berry, J. A.: Physiological and environmental regulation of stomatal conductance, photosynthesis and transpiration: a model that includes a laminar boundary layer, Agricultural and Forest Meteorology, 54(2–4), 107–136, doi:10.1016/0168-1923(91)90002-8, 1991.

Eamus, D., Hatton, T., Cook, P. and Colvin, C.: Ecohydrology: vegetation function, water and resource management, CSIRO Publishing, Collingwood VIC 3066., 2006.

Eamus, D., Cleverly, J., Boulain, N., Grant, N., Faux, R. and Villalobos-Vega, R.: Carbon and water fluxes in an arid-zone Acacia savanna woodland: An analyses of seasonal patterns and responses to rainfall events, Agricultural and Forest Meteorology, 182-183(3-4), 225–238, doi:10.1016/j.agrformet.2013.04.020, 2013.

Ehleringer, J. R., Cerling, T. E. and Helliker, B. R.: C4 photosynthesis, atmospheric CO2, and climate, Oecologia, 112, 285–299, 1997.

Falge, E., Baldocchi, D., Olson, R., Anthoni, P., Aubinet, M., Bernhofer, C., Burba, G., Ceulemans, R., Clement, R., Dolman, H., Granier, A., Gross, P., Grünwald, T., Hollinger, D., Jensen, N.-O., Katul, G., Keronen, P., Kowalski, A., Ta Lai, C., Law, B. E., Meyers, T., Moncrieff, J., Moors, E., William Munger, J., Pilegaard, K., Rannik, Ü., Rebmann, C., Suyker, A., Tenhunen, J., Tu, K., Verma, S., Vesala, T., Wilson, K. and Wofsy, S.: Gap filling strategies for long term energy flux data sets, Agricultural and Forest Meteorology, 107(1), 71–77, doi:10.1016/S0168-1923(00)00235-5, 2001.

Fasullo, J. T., Boening, C., Landerer, F. W. and Nerem, R. S.: Australia's unique influence on global sea level in 2010–2011, Geophys. Res. Lett., 40(16), 4368–4373, doi:10.1002/grl.50834, 2013.

Gamon, J. A., Huemmrich, K. F., Stone, R. S. and Tweedie, C. E.: Spatial and temporal variation in primary productivity (NDVI) of coastal Alaskan tundra: Decreased vegetation growth following earlier snowmelt, Remote Sensing of Environment, 129, 144–153, doi:10.1016/j.rse.2012.10.030, 2013.

Gao, X., Huete, A. R., Ni, W. and Miura, T.: Optical–Biophysical Relationships of Vegetation Spectra without Background Contamination, Remote Sensing of Environment, 74(3), 609–620, doi:10.1016/S0034-4257(00)00150-4, 2000.

Gesch, D. B., Verdin, K. L. and Greenlee, S. K.: New land surface digital elevation model covers the Earth, Eos Trans. AGU, 80(6), 69–70, doi:10.1029/99EO00050, 1999.

Van Gorsel, E.: Impact of the 2012-2013 summer heat records on forest productivity in eastern Australia, Biogeosciences, in this issue.

Van Gorsel, E., Berni, J. A. J., Briggs, P., Cabello-Leblic, A., Chasmer, L., Cleugh, H. A., Hacker, J., Hantson, S., Haverd, V., Hughes, D., Hopkinson, C., Keith, H., Kljun, N., Leuning, R., Yebra, M. and Zegelin, S.: Primary and secondary effects of climate variability on net ecosystem carbon exchange in an evergreen Eucalyptus forest, Agricultural and Forest Meteorology, 182-183, 248–256, doi:10.1016/j.agrformet.2013.04.027, 2013.

Hill, M. J., Held, A. A., Leuning, R., Coops, N. C., Hughes, D. and Cleugh, H. A.: MODIS spectral signals at a flux tower site: Relationships with high-resolution data, and CO2 flux and light use efficiency measurements, Remote Sensing of Environment, 103(3), 351–368, doi:10.1016/j.rse.2005.06.015, 2006.

Huete, A., Justice, C. and Liu, H.: Development of vegetation and soil indices for MODIS-EOS, Remote Sensing of Environment, 49(3), 224–234, doi:10.1016/0034-4257(94)90018-3, 1994.

Huete, A., Didan, K., Miura, T., Rodriguez, E. P., Gao, X. and Ferreira, L. G.: Overview of the radiometric and biophysical performance of the MODIS vegetation indices, Remote Sensing of Environment, 83(1–2), 195–213, doi:10.1016/S0034-4257(02)00096-2, 2002.

Huete, A., Restrepo-Coupe, N., Ratana, P., Didan, K., Saleska, S., Ichii, K., Panuthai, S. and Gamo, M.: Multiple site tower flux and remote sensing comparisons of tropical forest dynamics in Monsoon Asia, Agricultural and Forest Meteorology, 148(5), 748–760, doi:10.1016/j.agrformet.2008.01.012, 2008.

Huete, A. R.: A soil-adjusted vegetation index (SAVI), Remote Sensing of Environment, 25(3), 295–309, doi:10.1016/0034-4257(88)90106-X, 1988.

Huete, A. R. and Tucker, C. J.: Investigation of soil influences in AVHRR red and near-infrared vegetation index imagery, International Journal of Remote Sensing, 12(6), 1223–1242, doi:10.1080/01431169108929723, 1991.

Huete, A. R., Didan, K., Shimabukuro, Y. E., Ratana, P., Saleska, S. R., Hutyra, L. R., Yang, W., Nemani, R. R. and Myneni, R.: Amazon rainforests green-up with sunlight in dry season, Geophys. Res. Lett., 33, L06405, doi:200610.1029/2005GL025583, 2006.

Huffman, G. J., Bolvin, D. T., Nelkin, E. J., Wolff, D. B., Adler, R. F., Gu, G., Hong, Y., Bowman, K. P. and Stocker, E. F.: The TRMM Multisatellite Precipitation Analysis (TMPA): Quasi-Global, Multiyear, Combined-Sensor Precipitation Estimates at Fine Scales, J. Hydrometeor, 8(1), 38–55, doi:10.1175/JHM560.1, 2007.

Hutley, L. B., O’Grady, A. P. and Eamus, D.: Evapotranspiration from Eucalypt open-forest savanna of Northern Australia, Functional Ecology, 14(2), 183–194, doi:10.1046/j.1365-2435.2000.00416.x, 2000.

Hutley, L. B., Beringer, J., Isaac, P. R., Hacker, J. M. and Cernusak, L. A.: A sub-continental scale living laboratory: Spatial patterns of savanna vegetation over a rainfall gradient in northern Australia, Agricultural and Forest Meteorology, 151(11), 1417–1428, doi:10.1016/j.agrformet.2011.03.002, 2011.

Hutyra, L. R., Munger, J. W., Saleska, S. R., Gottlieb, E., Daube, B. C., Dunn, A. L., Amaral, D. F., de Camargo, P. B. and Wofsy, S. C.: Seasonal controls on the exchange of carbon and water in an Amazonian rain forest, Journal of Geophysical Research: Biogeosciences, 112(G3), G03008 , doi:10.1029/2006JG000365, 2007.

Isaac, P., Cleverly, J., Beringer, J. and McHugh, I.: The OzFlux Network Data Path: From Collection to Curation, Biogeosciences, in this issue.

Johnson, K. A. and Goody, R. S.: The Original Michaelis Constant: Translation of the 1913 Michaelis–Menten Paper, Biochemistry, 50(39), 8264–8269, doi:10.1021/bi201284u, 2011.

Kanniah, K. D., Beringer, J., Hutley, L. B., Tapper, N. J. and Zhu, X.: Evaluation of Collections 4 and 5 of the MODIS Gross Primary Productivity product and algorithm improvement at a tropical savanna site in northern Australia, Remote Sensing of Environment, 113(9), 1808–1822, doi:10.1016/j.rse.2009.04.013, 2009.

Kanniah, K. D., Beringer, J. and Hutley, L. B.: Environmental controls on the spatial variability of savanna productivity in the Northern Territory, Australia, Agricultural and Forest Meteorology, 151(11), 1429–1439, doi:10.1016/j.agrformet.2011.06.009, 2011.

Kanniah, K. D., Beringer, J., North, P. and Hutley, L.: Control of atmospheric particles on diffuse radiation and terrestrial plant productivity A review, Progress in Physical Geography, 36(2), 209–237, doi:10.1177/0309133311434244, 2012.

Kanniah, K. D., Beringer, J. and Hutley, L.: Exploring the link between clouds, radiation, and canopy productivity of tropical savannas, Agricultural and Forest Meteorology, 182-183, 304–313, doi:10.1016/j.agrformet.2013.06.010, 2013.

Kato, S., Loeb, N. G., Rose, F. G., Doelling, D. R., Rutan, D. A., Caldwell, T. E., Yu, L. and Weller, R. A.: Surface Irradiances Consistent with CERES-Derived Top-of-Atmosphere Shortwave and Longwave Irradiances, J. Climate, 26(9), 2719–2740, doi:10.1175/JCLI-D-12-00436.1, 2012.

Knyazikhin, Y., Glassy, J., Privette, J. L., Tian, Y., Lotsch, A., Zhang, Y., Wang, Y., Morisette, J. T., Votava, P., Myneni, R. B., Nemani, R. R. and Running, S. W.: MODIS Leaf Area Index (LAI) and Fraction of Photosynthetically Active Radiation Absorbed by Vegetation (FPAR) Product (MOD15): Algorithm Theoretical Basis Document, , available at: http:

//modis.gsfc.nasa.gov/data/atbd/atbd_mod15.pdf (last access: 20 December 2012), NASA, Earth Observing System Group, Greenbelt, MD, USA, 1999.

Koerber, G. R., Cleverly, J., Isaac, P. and Meyer, W. S.: Use of light-use efficiency functions to describe CO2 uptake at a semi-arid site, role of leaf-area index and leaf density, methods of estimating ecosystem respiration using LUE curves, Biogeosciences, in this issue.

Kottek, M., Grieser, J., Beck, C., Rudolf, B. and Rubel, F.: World Map of the Köppen-Geiger climate classification updated, Meteorologische Zeitschrift, 15(3), 259–263, doi:10.1127/0941-2948/2006/0130, 2006.

Leuning, R., Cleugh, H. A., Zegelin, S. J. and Hughes, D.: Carbon and water fluxes over a temperate Eucalyptus forest and a tropical wet/dry savanna in Australia: measurements and comparison with MODIS remote sensing estimates, Agricultural and Forest Meteorology, 129(3–4), 151–173, doi:10.1016/j.agrformet.2004.12.004, 2005.

Maeda, E. E., Heiskanen, J., Aragão, L. E. O. C. and Rinne, J.: Can MODIS EVI monitor ecosystem productivity in the Amazon rainforest?, Geophys. Res. Lett., 41(20), 2014GL061535, doi:10.1002/2014GL061535, 2014.

Mahadevan, P., Wofsy, S. C., Matross, D. M., Xiao, X., Dunn, A. L., Lin, J. C., Gerbig, C., Munger, J. W., Chow, V. Y. and Gottlieb, E. W.: A satellite-based biosphere parameterization for net ecosystem CO2 exchange: Vegetation Photosynthesis and Respiration Model (VPRM), Global Biogeochemical Cycles, 22(2), B2005, doi:10.1029/2006GB002735, 2008.

Ma, X., Huete, A., Yu, Q., Coupe, N. R., Davies, K., Broich, M., Ratana, P., Beringer, J., Hutley, L. B., Cleverly, J., Boulain, N. and Eamus, D.: Spatial patterns and temporal dynamics in savanna vegetation phenology across the North Australian Tropical Transect, Remote Sensing of Environment, 139(0), 97–115, doi:10.1016/j.rse.2013.07.030, 2013.

Ma, X., Huete, A., Yu, Q., Restrepo-Coupe, N., Beringer, J., Hutley, L. B., Kanniah, K. D., Cleverly, J. and Eamus, D.: Parameterization of an ecosystem light-use-efficiency model for predicting savanna GPP using MODIS EVI, Remote Sensing of Environment, 154, 253–271, doi:10.1016/j.rse.2014.08.025, 2014.

Meyer, W. S., Kondrlovà, E. and Koerber, G. R.: Evaporation of perennial semi-arid woodland in southeastern Australia is adapted for irregular but common dry periods, Hydrol. Process., 29, Issue 17, 3714–3726, doi:10.1002/hyp.10467, 2015.

Michaelis, L. and Menten, M. L.: Die Kinetik der Invertinwirkung, Biochemistry, 49, 333–369, 1913.

TRMM: Tropical Rainfall Measuring Mission Project, 3B43: Monthly 0.25 × 0.25 merged TRMM and other estimates v7, NASA Distrib. Active Arch. Cent., NASA, Goddard Space Flight Cent. Earth Sci., Greenbelt, MD, USA, available at: http://mirador.gsfc.nasa.gov/collections/TRMM_3B43__007.shtml (last access: 27 February 2014), 2014b.

van Niel, T. G., McVicar, T. R., Roderick, M. L., van Dijk, A. I. J. M., Beringer, J., Hutley, L. B. and van Gorsel, E.: Upscaling latent heat flux for thermal remote sensing studies: Comparison of alternative approaches and correction of bias, Journal of Hydrology, 468–469, 35–46, doi:10.1016/j.jhydrol.2012.08.005, 2012.

Olofsson, P., Lagergren, F., Lindroth, A., Lindström, J., Klemedtsson, L., Kutsch, W. and Eklundh, L.: Towards operational remote sensing of forest carbon balance across Northern Europe, Biogeosciences, 5(3), 817–832, doi:10.5194/bg-5-817-2008, 2008.

Papaioannou, G., Papanikolaou, N. and Retalis, D.: Relationships of photosynthetically active radiation and shortwave irradiance, Theoretical and Applied Climatology, 48(1), 23–27, doi:10.1007/BF00864910, 1993.

Papale, D., Reichstein, M., Aubinet, M., Canfora, E., Bernhofer, C., Kutsch, W., Longdoz, B., Rambal, S., Valentini, R., Vesala, T. and Yakir, D.: Towards a standardized processing of Net Ecosystem Exchange measured with eddy covariance technique: Algorithms and uncertainty estimation, Biogeosciences, 3(4), 571–583, 2006.

Peng, Y. and Gitelson, A. A.: Remote estimation of gross primary productivity in soybean and maize based on total crop chlorophyll content, Remote Sensing of Environment, 117, 440–448, doi:10.1016/j.rse.2011.10.021, 2012.

Poulter, B., Frank, D., Ciais, P., Myneni, R. B., Andela, N., Bi, J., Broquet, G., Canadell, J. G., Chevallier, F., Liu, Y. Y., Running, S. W., Sitch, S. and van der Werf, G. R.: Contribution of semi-arid ecosystems to interannual variability of the global carbon cycle, Nature, 509(7502), 600–603, doi:10.1038/nature13376, 2014.

Restrepo-Coupe, N., Rocha, H. R. da, Christoffersen, B., Araujo, A. C. da, Borma, L. S., Cabral, O. M. R., Camargo, P. B. de, Cardoso, F. L., Costa, A. C. L. da, Fitzjarrald, D. R., Goulden, M. L., Hutyra, L. R., Kruijt, B., Maia, J. M. F., Malhi, Y. S., Manzi, A. O., Miller, S. D., Nobre, A. D., Randow, C. von, Sá, L. D. da A., Sakai, R. K., Tota, J., Wofsy, S. C., Zanchi, F. B. and Saleska, S. R.: What drives the seasonality of productivity across the Amazon basin? A cross-site analysis of eddy flux tower measurements from the Brasil flux network, Agricultural and Forest Meteorology, 182– 183, 128– 144, 2013.

Richardson, A. D. and Hollinger, D. Y.: Statistical modeling of ecosystem respiration using eddy covariance data: Maximum likelihood parameter estimation, and Monte Carlo simulation of model and parameter uncertainty, applied to three simple models, Agricultural and Forest Meteorology, 131(3-4), 191–208, doi:10.1016/j.agrformet.2005.05.008, 2005.

Rubel, F. and Kottek, M.: Observed and projected climate shifts 1901–2100 depicted by world maps of the Köppen-Geiger climate classification, Meteorologische Zeitschrift, 19(2), 135–141, doi:10.1127/0941-2948/2010/0430, 2010.

Running, S. W., Justice, C. O., Salomonson, V., Hall, D., Barker, J., Kaufmann, Y. J., Strahler, A. H., Huete, A. R., Muller, J.-P., Vanderbildt, V., Wan, Z. M., Teillet, P. and Carneggie, D.: Terrestrial remote sensing science and algorithms planned for EOS/MODIS, International Journal of Remote Sensing, 15(17), 3587–3620, doi:10.1080/01431169408954346, 1994.

Running, S. W., Thornton, P. E., Nemani, R. and Glassy, J. M.: Global terrestrial gross and net primary productivity from the Earth Observing System, Methods in ecosystem science, Springer New York, USA, 44–57, 2000.

Santin-Janin, H., Garel, M., Chapuis, J.-L. and Pontier, D.: Assessing the performance of NDVI as a proxy for plant biomass using non-linear models: a case study on the Kerguelen archipelago, Polar Biol, 32(6), 861–871, doi:10.1007/s00300-009-0586-5, 2009.

Schaaf, C. B., Gao, F., Strahler, A. H., Lucht, W., Li, X., Tsang, T., Strugnell, N. C., Zhang, X., Jin, Y., Muller, J.-P., Lewis, P., Barnsley, M., Hobson, P., Disney, M., Roberts, G., Dunderdale, M., Doll, C., d'Entremont, R. P., Hu, B., Liang, S., Privette, J. L. and Roy, D.: First operational BRDF, albedo nadir reflectance products from MODIS, Remote Sensing of Environment, 83(1–2), 135–148, doi:10.1016/S0034-4257(02)00091-3, 2002.

Shen, S. and Leptoukh, G. G.: Estimation of surface air temperature over central and eastern Eurasia from MODIS land surface temperature, Environ. Res. Lett., 6(4), 045206, doi:10.1088/1748-9326/6/4/045206, 2011.

Sims, D. A., Rahman, A. F., Cordova, V. D., El-Masri, B. Z., Baldocchi, D. D., Flanagan, L. B., Goldstein, A. H., Hollinger, D. Y., Misson, L., Monson, R. K., Oechel, W. C., Schmid, H. P., Wofsy, S. C. and Xu, L.: On the use of MODIS EVI to assess gross primary productivity of North American ecosystems, J. Geophys. Res., 111(G4), G04015, doi:10.1029/2006JG000162, 2006.

Sims, D. A., Rahman, A. F., Cordova, V. D., El-Masri, B. Z., Baldocchi, D. D., Bolstad, P. V., Flanagan, L. B., Goldstein, A. H., Hollinger, D. Y., Misson, L., Monson, R. K., Oechel, W. C., Schmid, H. P., Wofsy, S. C. and Xu, L.: A new model of gross primary productivity for North American ecosystems based solely on the enhanced vegetation index and land surface temperature from MODIS, Remote Sensing of Environment, 112(4), 1633–1646, doi:10.1016/j.rse.2007.08.004, 2008.

Sjöström, M., Ardö, J., Arneth, A., Boulain, N., Cappelaere, B., Eklundh, L., de Grandcourt, A., Kutsch, W. L., Merbold, L., Nouvellon, Y., Scholes, R. J., Schubert, P., Seaquist, J. and Veenendaal, E. M.: Exploring the potential of MODIS EVI for modeling gross primary production across African ecosystems, Remote Sensing of Environment, 115(4), 1081–1089, doi:10.1016/j.rse.2010.12.013, 2011.

Stoy, P. C., Katul, G. G., Siqueira, M. B. S., Juang, J.-Y., Novick, K. A., Uebelherr, J. M. and Oren, R.: An evaluation of models for partitioning eddy covariance-measured net ecosystem exchange into photosynthesis and respiration, Agricultural and Forest Meteorology, 141(1), 2–18, doi:doi: DOI: 10.1016/j.agrformet.2006.09.001, 2006.

Suyker, A. E. and Verma, S. B.: Year-round observations of the net ecosystem exchange of carbon dioxide in a native tallgrass prairie, Global Change Biology, 7(3), 279–289, doi:10.1046/j.1365-2486.2001.00407.x, 2001.

Szeicz, G.: Solar Radiation for Plant Growth, Journal of Applied Ecology, 11(2), 617–636, 1974.

Taylor, K. E.: Summarizing multiple aspects of model performance in a single diagram, J. Geophys. Res., 106(D7), PP. 7183–7192, doi:200110.1029/2000JD900719, 2001.

Tezara, W., Mitchell, V. J., Driscoll, S. D. and Lawlor, D. W.: Water stress inhibits plant photosynthesis by decreasing coupling factor and ATP, Nature, 401(6756), 914–917, doi:10.1038/44842, 1999.

Veroustraete, F., Sabbe, H. and Eerens, H.: Estimation of carbon mass fluxes over Europe using the C-Fix model and Euroflux data, Remote Sensing of Environment, 83(3), 376–399, doi:10.1016/S0034-4257(02)00043-3, 2002.

Vitasse, Y., Lenz, A. and Körner, C.: The interaction between freezing tolerance and phenology in temperate deciduous trees, Front Plant Sci, 5, 00541, doi:10.3389/fpls.2014.00541, 2014.

Wang, J., Rich, P. M., Price, K. P. and Kettle, W. D.: Relations between NDVI and tree productivity in the central Great Plains, International Journal of Remote Sensing, 25(16), 3127–3138, doi:10.1080/0143116032000160499, 2004.

Waring, H. R. and Running, W. S.: Forest Ecosystems: Analysis at Multiple Scales, Academic Press, San Diego, CA, USA., 1998.

Wofsy, S., Goulden, M. and Munger, J. W.: Net Exchange of CO2 in a Mid-Latitude Forest, Science, 260, 1314 – 1317, 1993.

Wohlfahrt, G., Gu, L., 2015. The many meanings of gross photosynthesis and their implication for photosynthesis research from leaf to globe. Plant Cell Environ. 38, 2500–2507. doi:10.1111/pce.12569

Wu, C., Niu, Z. and Gao, S.: Gross primary production estimation from MODIS data with vegetation index and photosynthetically active radiation in maize, J. Geophys. Res., 115(D12), D12127, doi:10.1029/2009JD013023, 2010.

Wu, C., Chen, J. M. and Huang, N.: Predicting gross primary production from the enhanced vegetation index and photosynthetically active radiation: Evaluation and calibration, Remote Sensing of Environment, 115(12), 3424–3435, doi:10.1016/j.rse.2011.08.006, 2011.

Xiao, X., Zhang, Q., Braswell, B., Urbanski, S., Boles, S., Wofsy, S., Moore III, B. and Ojima, D.: Modeling gross primary production of temperate deciduous broadleaf forest using satellite images and climate data, Remote Sensing of Environment, 91(2), 256–270, doi:10.1016/j.rse.2004.03.010, 2004.

Zolfaghar, S.: Comparative ecophysiology of Eucalyptus woodlands along a depth-to-groundwater gradient, PhD thesis, University Technology of Sydney, Sydney, Australia, 1 September., 2013.

List of tables

Table *1*. OzFlux sites presented in this study -location and additional information.

Table *2*. Remote sensing data sources, cell size, sample size (eddy-covariance tower-site at the centre pixel) and time interval.

Table *3*. Linear regressions obtained by a nonlinear mixed-effects regression model for gross ecosystem productivity (*GEP*, gC m^{-2} d^{-1}) versus combinations of 16-day average MODIS products: fixed solar zenith angle of 30˚ enhanced vegetation index (EVI_{SZA30}), daytime and land surface temperature (LST_{day}, °C), fixed solar zenith angle of 30˚ normalized difference vegetation index ($NDVI_{SZA30}$), precipitation from the Tropical Rainfall Measuring Mission ($Precip_{TRMM}$, mm $month^{-1}$) data product from 1998-2013 (TRMM, 2014), and surface shortwave incident radiation from the Clouds and the Earth's Radiant Energy System (SW_{CERES}, W m^{-2}) data product from 2000–2013 (CERES, 2014). Model runs for AU-How: Howard Springs, AU-ASM: Alice Springs Mulga, AU-Cpr: Calperum-Chowilla, and AU-Tum: Tumbarumba, and all available data (includes all sites). Bold fonts highlight values mentioned on the text.

List of figures

Figure 1. Location of four OzFlux eddy covariance tower sites included on this analysis: AU-How: Howard Springs (at Aw), AU-ASM: Alice Springs Mulga (at boundary BSh and BWh), AU-Cpr: Calperum-Chowilla (at Bwk), and AU-Tum: Tumbarumba (at boundary Cfa and Cfb). Köppen-Geiger climate classification as published by Kottek et al. (2006) and Rubel and Kottek (2010). Where Aw is equatorial winter dry climate, BSh is arid steppe, BWh is hot arid desert, BWk is cold arid desert, Cfb is warm temperate fully humid warm summer, Cfa is warm temperate fully humid hot summer and Cwa is warm temperate winter dry hot summer.

Figure 2. Rectangular hyperbola fitted to 16-day worth of hourly gross ecosystem productivity (*GEP*, μmolCO_2 m^{-2} s^{-1}) versus photosynthetic active radiation (PAR, μmol m^{-2} s^{-1}) data measured at Howard Springs eddy covariance tower (black line). From the rectangular hyperbola: quantum yield (α, μmolCO_2 $μmol^{-1}$) (blue dashed line) and GEP at saturation (GEP_{sat}, μmolCO_2 m^{-2} s^{-1}) (blue doted line). Photosynthetic capacity (Pc, μmolCO_2 m^{-2} s^{-1}) (black dashed line) was calculated as the 16-day mean GEP at mean annual daytime PAR ($\overline{PAR}$) ±100 μmol m^{-2} s^{-1} (grey area) and mean annual VPD ($\overline{VPD}$) ±2 standard deviations. Light use efficiency (LUE, μmolCO_2 $μmol^{-1}$) was defined as the ratio between daily GEP over PAR, the slope of the linear regression (blue line).

Figure 3. Savanna (AU-How), wet sclerophyll (AU-Tum), Mulga (AU-ASM), and Mallee (AU-Cpr) ecosystems, OzFlux sites annual cycle (16-day composites) of (a) precipitation (*Precip*; mm $month^{-1}$) (grey bars) and photosynthetic active radiation (PAR; μmol m^{-2} d^{-1}) (blue line), and (b) vapour pressure deficit (*VPD*; kPa) (black line) and air temperature (T_{air}; ˚C) (blue line). Grey boxes indicate Southern Hemisphere spring and summer September to March.

Figure 4. Savanna (AU-How), wet sclerophyll (AU-Tum) , Mulga (AU-ASM), and Mallee (AU-Cpr) ecosystems, OzFlux sites annual cycle (16-day composites) of eddy flux derived (a) Gross Ecosystem Productivity (*GEP*; gC m^{-2} d^{-1}) (black line) and MODIS Gross Primary Productivity (GPP_{MOD}) product (light blue line); (b) *GEP* at saturation light (GEP_{sat}; gC m^{-2} d^{-1}) (black line) and ecosystem quantum yield (α; gC MJ^{-1}) (light blue line); (c) photosynthetic capacity (*Pc*; gC m^{-2} d^{-1}) (black line) and the ratio of *GEP* over *PAR* (black line), the light use efficiency (*LUE*; gC MJ^{-1}) (light blue line). At the bottom two panels, satellite derived data of: (d) MODIS Enhanced Vegetation Index at fixed solar zenith angle of 30˚ (EVI_{SZA30}) (black line) and the Normalized Difference Vegetation Index ($NDVI_{SZA30}$) (light blue line); (e) MODIS Leaf Area Index (LAI_{MOD}) (black line) and MODIS Fraction of the Absorbed Photo-synthetic Active Radiation ($fPAR_{MOD}$) (light blue line). Grey boxes indicate Southern Hemisphere spring and summer September to March. Black dashed vertical line indicates the timing of maximum *GEP*.

Figure 5. Top row: Linear regression between 16 and 8-day time series of measured gross ecosystem productivity (*GEP*; gC m^{-2} d^{-1}) (top row) and the MODIS fixed solar zenith angle of 30˚ enhanced ve-

getation index (EVI_{SZA30}) at (a) Howard Springs (AU-How) open woodland savanna, (b) Alice Springs Mulga (AU-ASM), (c) Tumbarumba (AU-Tum) wet sclerophyll forest eddy, and (d) Chowilla Mallee (AU-Cpr) covariance site. Lower row: Regression between *GEP* and MODIS gross primary productivity (GPP_{MOD}) (e) AU-How, (f) AU-Tum, (g) AU-ASM, and (h) AU-Cpr.

Figure 6. Relationships between 16-day mean values of (a) light use efficiency (*LUE*; gC MJ^{-1}), (b) photosynthetic capacity (*Pc*; gC m^{-2} d^{-1}), (c) ecosystem quantum yield (α; gC MJ^{-1}), and (d) *GEP* at saturation light (GEP_{sat}; gC m^{-2} d^{-1}), and MODIS fixed solar zenith angle of 30˚ enhanced vegetation index (EVI_{SZA30}). Four key Australian ecosystem sites, from left to right (columns), AU-How savanna, AU-ASM Mulga, wet sclerophyll forest of AU-Tum and AU-Cpr Mallee.

Figure 7. Taylor diagrams showing model results for Howard Springs (AU-How), Tumbarumba (AU-Tum), Alice Springs (AU-ASM) and Calperum-Chowilla (AU-Cpr) based on site-specific and all sites linear regressions between gross ecosystem productivity (*GEP*), light use efficiency (*LUE*), photosynthetic capacity (*Pc*) and ecosystem quantum yield (*α*) and different remote sensing products MODIS fixed solar zenith angle of 30˚ Enhanced Vegetation Index (*EVI*) and Normalized Difference Vegetation Index (*NDVI*), Gross Primary Productivity product (*GPP*), daytime Land surface Temperature (*LST*), Leaf Area Index (*LAI*), fraction of the absorbed Photosynthetic Active Radiation (*fPAR*). All site relationships is labelled with an asterisk (e.g. *EVI**). *EVI* and *NDVI* labels are used instead of EVI_{SZA30} and $NDVI_{SZA30}$ for displaying purposes. Missing sites indicate that the model overestimates the seasonality of observations -model normalized standard deviation is >2.

Figure 8. Relationships between 16-day mean values of photosynthetic capacity (*Pc*; gC m^{-2} d^{-1}) and different RS products: (a) MODIS fixed solar zenith angle of 30˚ enhanced vegetation index (EVI_{SZA30}), (b) normalized difference vegetation index ($NDVI_{SZA30}$), (c) MODIS gross primary productivity (GPP_{MOD}; gC m^{-2} d^{-1}), (d) leaf area index (LAI_{MOD}), and (e) fraction of the absorbed photosynthetic active radiation ($fPAR_{MOD}$). Four key Australian ecosystem sites included on the analysis: AU-How savanna (blue circles), AU-ASM Mulga (yellow square markers), AU-Cpr Mallee (red triangles) and wet sclerophyll forest of AU-Tum (green diamonds).

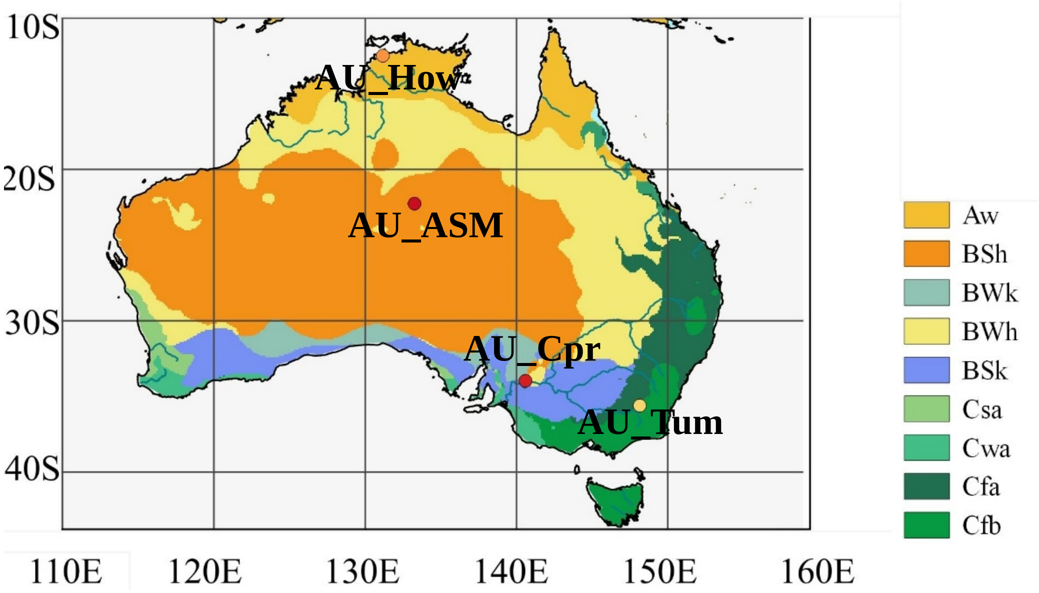

Figure 1. Location of four OzFlux eddy covariance tower sites included on this analysis: AU-How: Howard Springs (at Aw), AU-ASM: Alice Springs Mulga (at boundary BSh and BWh), AU-Cpr: Calperum-Chowilla (at Bwk), and AU-Tum: Tumbarumba (at boundary Cfa and Cfb). Köppen-Geiger climate classification as published by Kottek et al. (2006) and Rubel and Kottek (2010). Where Aw is equatorial winter dry climate, BSh is arid steppe, BWh is hot arid desert, BWk is cold arid desert, Cfb is warm temperate fully humid warm summer, Cfa is warm temperate fully humid hot summer and Cwa is warm temperate winter dry hot summer.

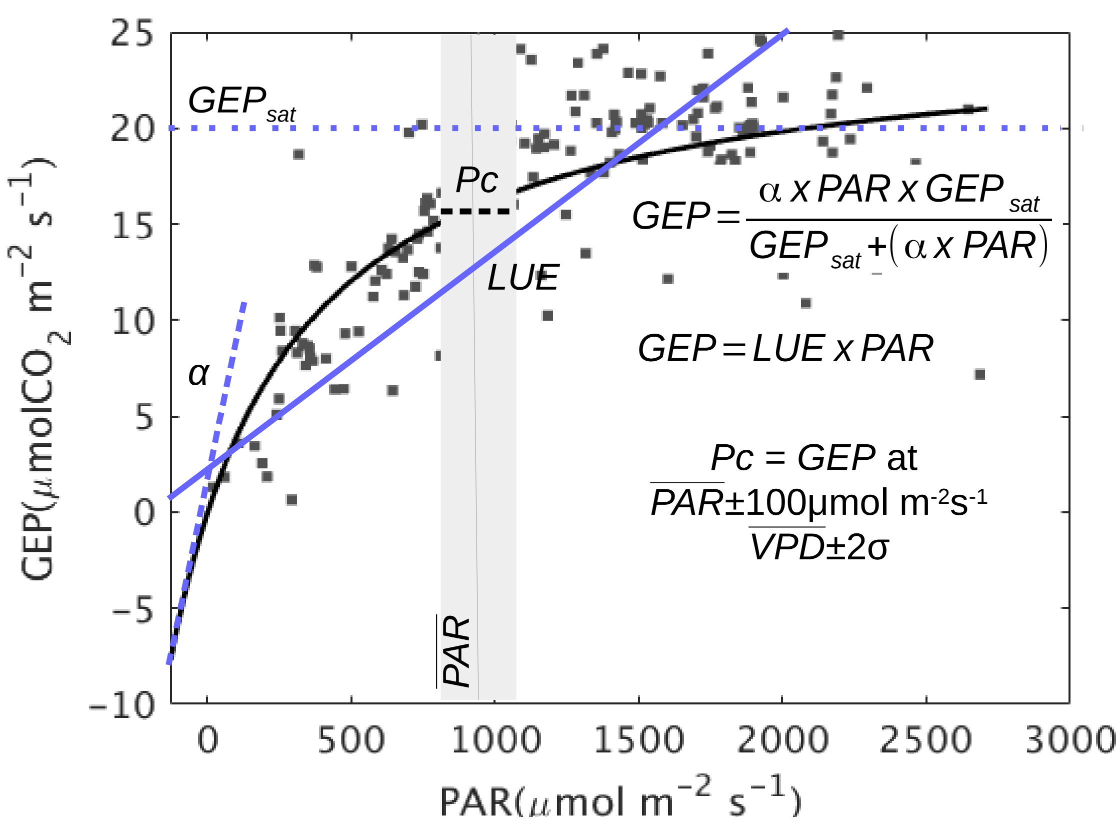

Figure 2. Rectangular hyperbola fitted to 16-day worth of hourly gross ecosystem productivity (*GEP*, μmolCO_2 m^{-2} s^{-1}) versus photosynthetic active radiation (PAR, μmol m^{-2} s^{-1}) data measured at Howard Springs eddy covariance tower (black line). From the rectangular hyperbola: quantum yield (α, μmolCO_2 μmol^{-1}) (blue dashed line) and GEP at saturation (GEP_{sat}, μmolCO_2 m^{-2} s^{-1}) (blue doted line). Photosynthetic capacity (Pc, μmolCO_2 m^{-2} s^{-1}) (black dashed line) was calculated as the 16-day mean GEP at mean annual daytime PAR ($\overline{PAR}$) ±100 μmol m^{-2} s^{-1} (grey area) and mean annual VPD ($\overline{VPD}$) ±2 standard deviations. Light use efficiency (LUE, μmolCO_2 μmol^{-1}) was defined as the ratio between daily GEP over PAR, the slope of the linear regression (blue line).

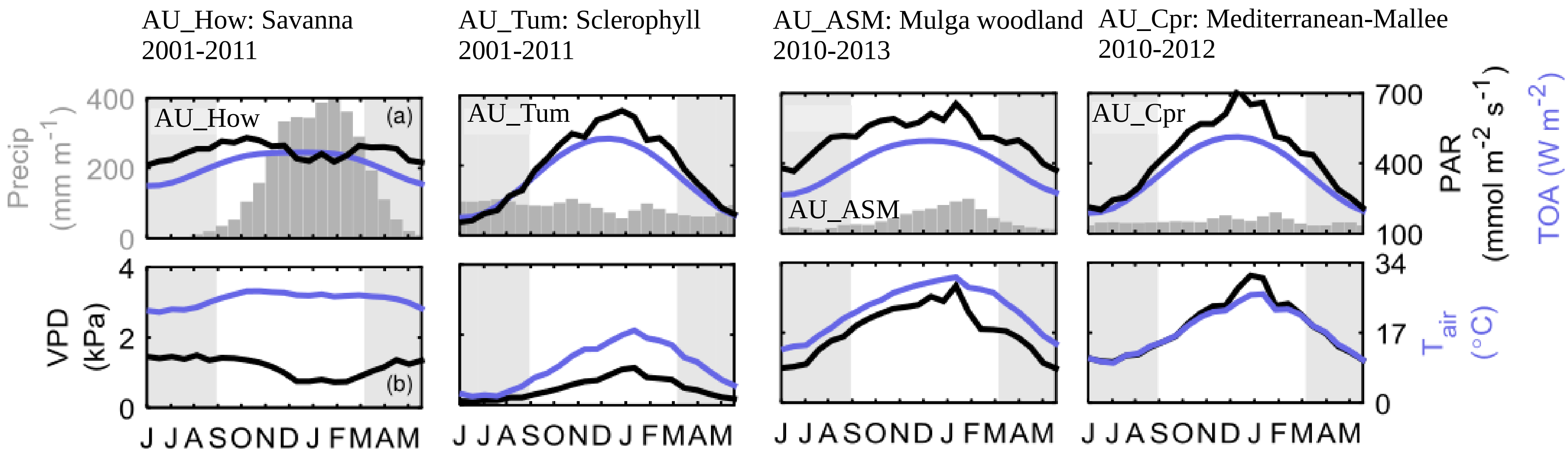

Figure 3. Savanna (AU-How), wet sclerophyll (AU-Tum), Mulga (AU-ASM), and Mallee (AU-Cpr) ecosystems, OzFlux sites annual cycle (16-day composites) of (a) precipitation (*Precip*; mm month^{-1}) (grey bars) and photosynthetic active radiation (PAR; µmol m^{-2} d^{-1}) (blue line), and (b) vapour pressure deficit (*VPD*; kPa) (black line) and air temperature (T_{air}; ˚C) (blue line). Grey boxes indicate Southern Hemisphere spring and summer September to March.

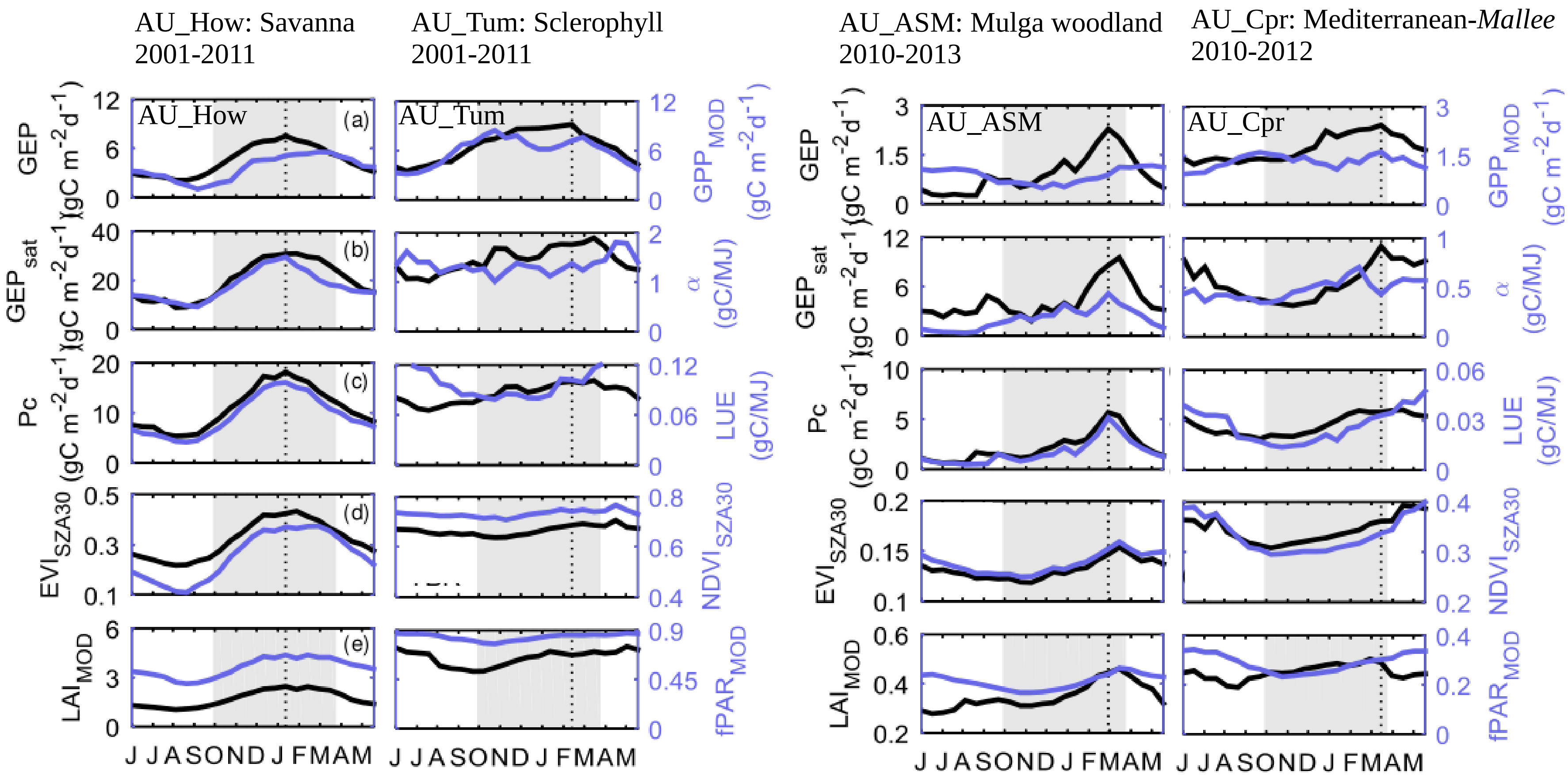

Figure 4. Savanna (AU-How), wet sclerophyll (AU-Tum) , Mulga (AU-ASM), and Mallee (AU-Cpr) ecosystems, OzFlux sites annual cycle (16-day composites) of eddy flux derived (a) Gross Ecosystem Productivity (*GEP*; gC m^{-2} d^{-1}) (black line) and MODIS Gross Primary Productivity (GPP_{MOD}) product (light blue line); (b) *GEP* at saturation light (GEP_{sat}; gC m^{-2} d^{-1}) (black line) and ecosystem quantum yield (α; gC MJ^{-1}) (light blue line); (c) photosynthetic capacity (*Pc*; gC m^{-2} d^{-1}) (black line) and the ratio of *GEP* over *PAR* (black line), the light use efficiency (*LUE*; gC MJ^{-1}) (light blue line). At the bottom two panels, satellite derived data of: (d) MODIS Enhanced Vegetation Index at fixed solar zenith angle of 30˚ (EVI_{SZA30}) (black line) and the Normalized Difference Vegetation Index ($NDVI_{SZA30}$) (light blue line); (e) MODIS Leaf Area Index (LAI_{MOD}) (black line) and MODIS Fraction of the Absorbed Photosynthetic Active Radiation ($fPAR_{MOD}$) (light blue line). Grey boxes indicate Southern Hemisphere spring and summer September to March. Black dashed vertical line indicates the timing of maximum *GEP*.

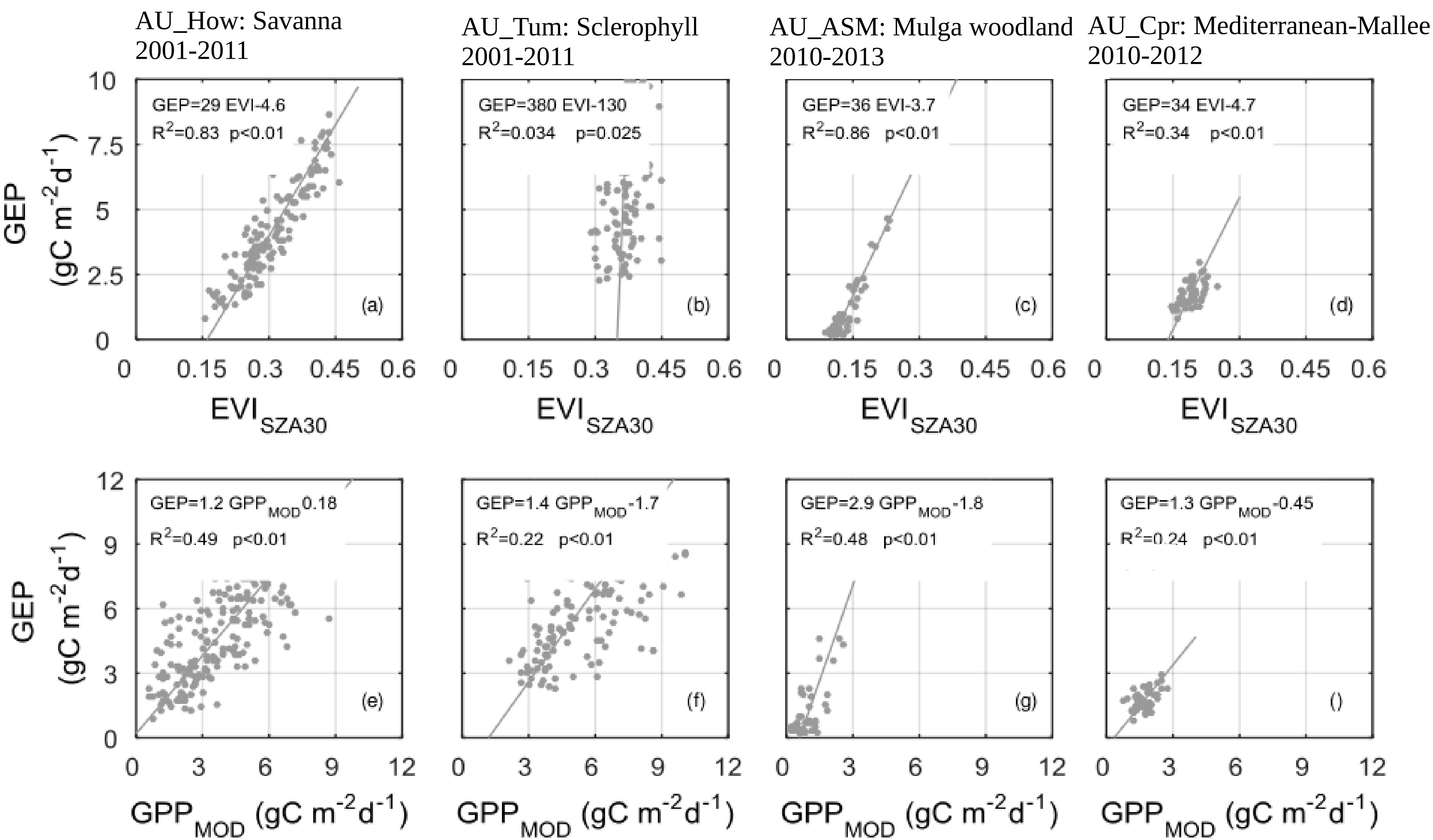

Figure 5. Top row: Linear regression between 16 and 8-day time series of measured gross ecosystem productivity (*GEP*; gC m^{-2} d^{-1}) (top row) and the MODIS fixed solar zenith angle of 30˚ enhanced vegetation index (EVI_{SZA30}) at (a) Howard Springs (AU-How) open woodland savanna, (b) Alice Springs Mulga (AU-ASM), (c) Tumbarumba (AU-Tum) wet sclerophyll forest eddy, and (d) Chowilla Mallee (AU-Cpr) covariance site. Lower row: Regression between *GEP* and MODIS gross primary productivity (GPP_{MOD}) (e) AU-How, (f) AU-Tum, (g) AU-ASM, and (h) AU-Cpr.

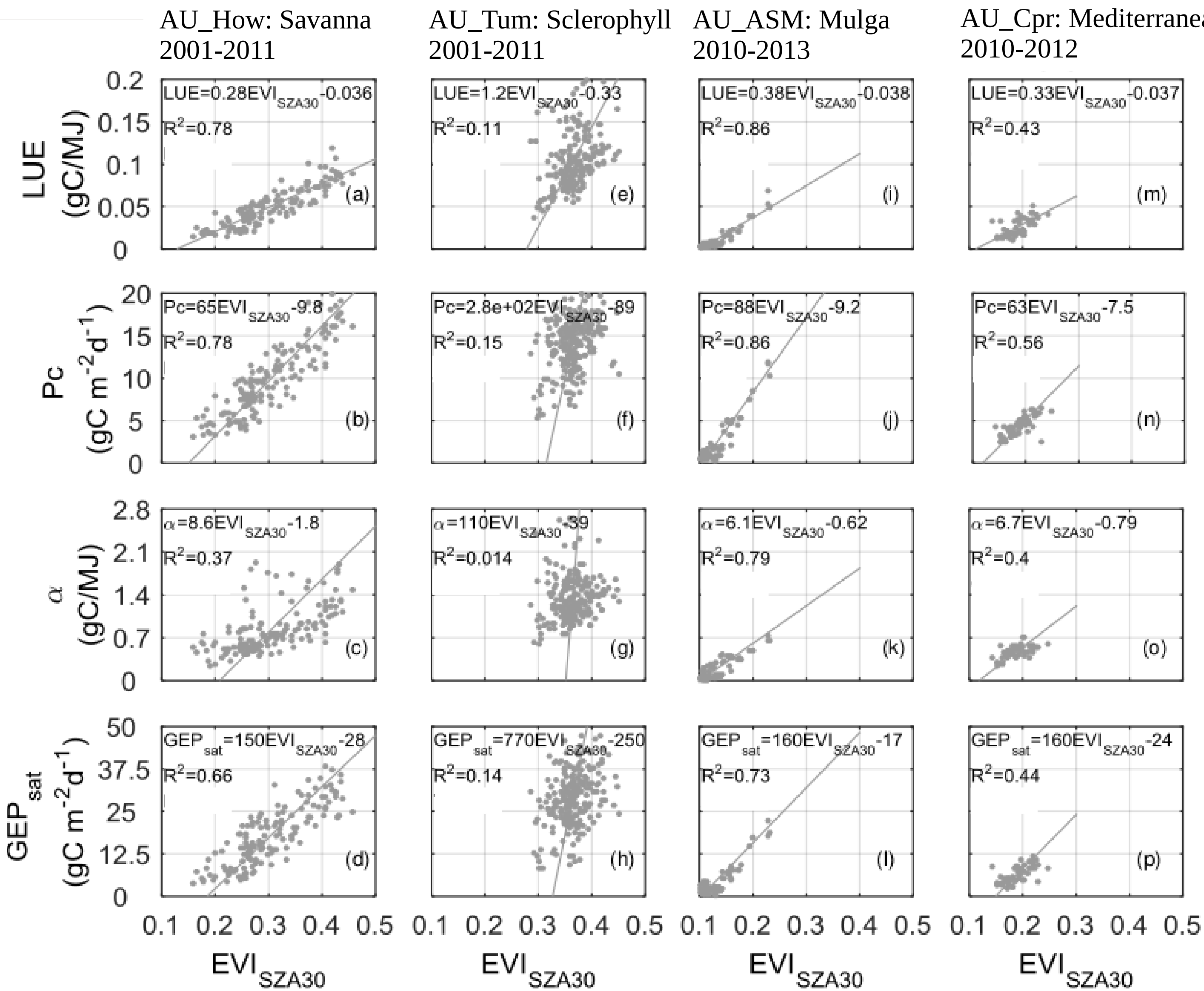

Figure 6. Relationships between 16-day mean values of (a) light use efficiency (*LUE*; gC MJ^{-1}), (b) photosynthetic capacity (*Pc*; gC m^{-2} d^{-1}), (c) ecosystem quantum yield (α; gC MJ^{-1}), and (d) *GEP* at saturation light (GEP_{sat}; gC m^{-2} d^{-1}), and MODIS fixed solar zenith angle of 30˚ enhanced vegetation index (EVI_{SZA30}). Four key Australian ecosystem sites, from left to right (columns), AU-How savanna, AU-ASM Mulga, wet sclerophyll forest of AU-Tum and AU-Cpr Mallee.

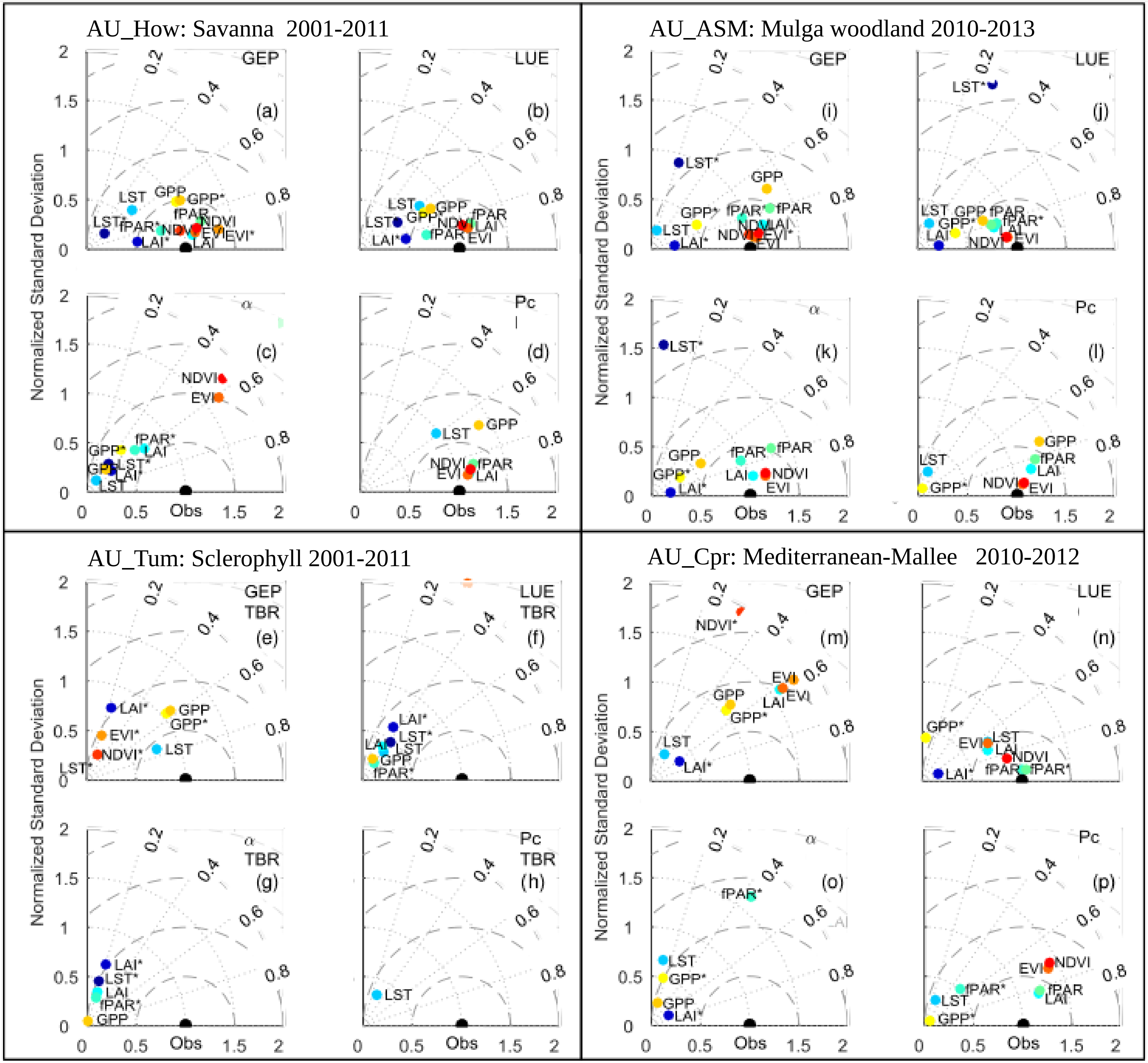

Figure 7. Taylor diagrams showing model results for Howard Springs (AU-How), Tumbarumba (AU-Tum), Alice Springs (AU-ASM) and Calperum-Chowilla (AU-Cpr) based on site-specific and all sites linear regressions between gross ecosystem productivity (*GEP*), light use efficiency (*LUE*), photosynthetic capacity (*Pc*) and ecosystem quantum yield (*α*) and different remote sensing products MODIS fixed solar zenith angle of 30˚ Enhanced Vegetation Index (*EVI*) and Normalized Difference Vegetation Index (*NDVI*), Gross Primary Productivity product (*GPP*), daytime Land surface Temperature (*LST*), Leaf Area Index (LAI), fraction of the absorbed Photosynthetic Active Radiation (*fPAR*). All site relationships is labelled with an asterisk (e.g. *EVI**). *EVI* and *NDVI* labels are used instead of EVI_{SZA30} and $NDVI_{SZA30}$ for displaying purposes. Missing sites indicate that the model overestimates the seasonality of observations -model normalized standard deviation is >2.

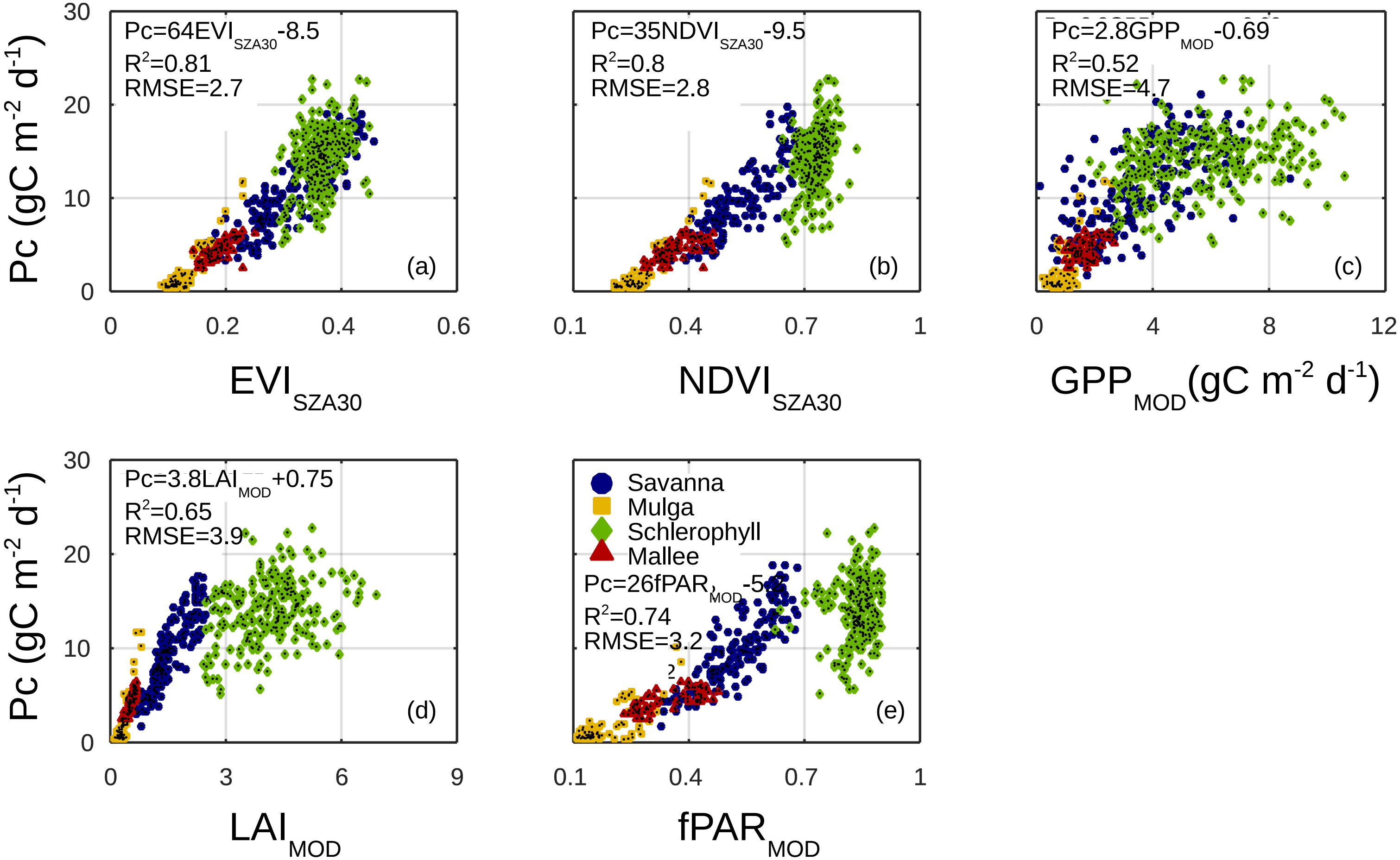

Figure 8. Relationships between 16-day mean values of photosynthetic capacity (*Pc*; gC m^{-2} d^{-1}) and different RS products: (a) MODIS fixed solar zenith angle of 30˚ enhanced vegetation index (EVI_{SZA30}), (b) normalized difference vegetation index ($NDVI_{SZA30}$), (c) MODIS gross primary productivity (GPP_{MOD}; gC m^{-2} d^{-1}), (d) leaf area index (LAI_{MOD}), and (e) fraction of the absorbed photosynthetic active radiation ($fPAR_{MOD}$). Four key Australian ecosystem sites included on the analysis: AU-How savanna (blue circles), AU-ASM Mulga (yellow square markers), AU-Cpr Mallee (red triangles) and wet sclerophyll forest of AU-Tum (green diamonds).

ID	Name	Measurement Period		Elevation	Lat/Lon		Vegetation Height	Biome	u*tresh	u*min	u*max
		Start	End	(m.a.s.l.)	(deg)		(m)		($m s^{-1}$)	($m s^{-1}$)	($m s^{-1}$)
AU_How	Howard Springs	2001	2015	64	-12.50	131.15	15	Open woodland savanna	0.122	0.000	0.253
AU_ASM	Alice Springs Mulga	2010	2013	606	-22.28	133.25	6	Mulga	0.105	0.000	0.215
AU_Tum	Tumbarumba	2001	2014	1200	-35.66	148.15	40	Wet sclerophyll forest	0.173	0.000	0.421
AU_Cpr	Calperum-Chowilla	2010	2012	379	-34.00	140.59	5	Malle	0.176	0.086	0.265

Table 1. OZflux sites presented in this study -location and additional information.

Product	Description	Data Source	Cell Size	Sample Size	Interval
LAI_{MOD}	Leaf Area Index	MOD15A2	1000 m	1x1	8 Day
$fPAR_{MOD}$	Fraction of Absorbed PAR	MOD15A2	1000 m	1x1	8 Day
LST_{day}	Daytime Land Surface Temperature	MOD11A2	1000 m	1x1	8 Day
GPP_{MOD}	Gross Primary Production	MOD17A2	1000 m	1x1	8 Day
EVI_{SZA30}	NBAR Enhanced Vegetation Index	MCD43A1	500 m	2x2	8 Day
$NDVI_{SZA30}$	NBAR Normalied Difference Vegetation Index	MCD43A1	500 m	2x2	8 Day
$TRMM$	Mean Monthly Precipitation	TRMM	0.25 degree	1x1	Monthly
SW_{CERES}	Short wave radiation	CERES	1 degree	1x1	Monthly

Table 2. Remote sensing data sources, cell size, sample size (eddy-covariance tower-site at the center pixel) and time interval.

	AU_How				AU_ASM				AU_Tum				AU_Cpr				All			
	Coeff [a b c d]	CI	R^2	AIC	Coeff	CI	R^2	AIC	Coeff	CI	R^2	AIC	Coeff	CI	R^2	AIC	Coeff	CI	R^2	AIC
GEP = a EVI + b	**[21.94 -2.65]**	**[0.96 0.28]**	**0.82**	**263**	**[26.01 -2.48]**	**[1.69 0.2]**	**0.85**	**64**	[15.52 0.90]	[5.55 2.01]	0.03	740	**[12.74 -0.71]**	**[2.05 0.38]**	**0.36**	**49**	**[22.47 -2.19]**	**[0.51 0.1]**	**0.69**	**1323**
GEP = a NDVI	[15.03 -4.11]	[0.70 0.35]	0.78	275	[14.34 -3.10]	[0.99 0.26]	0.83	80	[19.05 -7.28]	[5.23 3.79]	0.07	733	[3.97 0.24]	[1.29 0.46]	0.09	70	**[12.62 -2.74]**	**[0.27 0.12]**	**0.72**	**1276**
GEP = a LST_{day} + b	[-0.22 70.91]	[0.02 7.70]	0.28	676	[-0.02 7.59]	[0.013 3.90]	0.03	218	**[0.26 -68.09]**	**[0.015 4.45]**	**0.58**	**656**	[0.017 -3.27]	[0.006 1.74]	0.12	69	[-0.095 32.57]	[0.01 3.13]	0.14	2279
GEP = a $Precip_{TRMM}$ + b	[0.01 3.03]	[0.001 0.11]	0.53	627	[0.01 0.38]	[0.004 0.11]	0.30	182	[-0.017 7.54]	[0.005 0.31]	0.03	799	[0.0006 1.66]	[0.003 0.097]	0.02	73	[0.009 3.60]	[0.001 0.14]	0.13	2340
GEP = a SW_{CERES} + b	[-0.012 7.30]	[0.006 1.48]	0.02	781	[0.005 -0.30]	[0.002 0.59]	0.02	209	[0.026 1.025]	[0.001 0.26]	0.60	635	[0.003 1.14]	[0.0008 0.14]	0.12	67	[0.007 2.81]	[0.0016 0.32]	0.01	2329
GEP = a EVI + b LST_{day} + c LST_{day} EVI + d	[-29.96 127.38 0.09 -0.34]	[18.42 66.60 0.06 0.22]	0.82	268	[-11.51 76.94 0.03 -0.16]	[7.81 67.35 0.03 0.22]	0.87	66	[-2.64 1.38 0.08]	[0.21 10.71 0.04]	0.64	583	**[22.6 -145.8 -0.08 0.53]**	**[9.4 51.44 0.03 0.17]**	**0.63**	**30**	[-5.60 17.51 0.01 0.02]	[2.98 13.87 0.01 0.05]	0.70	1322
GEP = a EVI + b SW_{CERES} + c SW_{CERES} EVI + d	**[-3.57 24.15 0.003 -0.004]**	**[3.45 11.26 0.01 0.05]**	**0.82**	**266**	[2.48 -21.70 -0.02 0.19]	[0.99 8.68 0.004 0.03]	0.87	54	**[7.75 -19.41 -0.05 0.21]**	**[3.25 8.84 0.017 0.05]**	**0.70**	**553**	**[1.87 -4.52 -0.01 0.095]**	**[0.83 4.41 0.005 0.025]**	**0.62**	**26**	**[-0.31 4.95 -0.009 0.079]**	**[0.35 1.45 0.001 0.007]**	**0.82**	**1154**
GEP = a SW_{CERES} + b SW_{CERES} EVI + c	[3.63 -0.03 0.097]	[0.73 0.003 0.004]	0.82	263	**[-0.008 -0.01 0.10]**	**[0.18 0.001 0.006]**	**0.88**	**56**	[0.69 -0.014 0.12]	[0.29 0.006 0.016]	0.69	554	**[1.023 -0.01 0.07]**	**[0.097 0.001 0.008]**	**0.62**	**23**	[0.92 -0.014 0.1]	[0.13 0.001 0.002]	0.82	1179
GEP = a EVI + b $Precip_{TRMM}$ + c $Precip_{TRMM}$ EVI + d	**[-2.13 18.93 0.01 -0.02]**	**[0.34 1.28 0.004 0.01]**	**0.84**	**253**	**[-1.32 15.09 -0.019 0.18]**	**[0.25 2.19 0.005 0.04]**	**0.88**	**42**	[1.63 15.31 0.002 -0.04]	[3.78 10.29 0.06 0.16]	0.04	732	[0.21 6.96 -0.03 0.2]	[0.69 3.57 0.015 0.08]	0.52	43	[-2.35 22.48 0.008 -0.02]	[0.14 0.64 0.003 0.009]	0.66	1312
GEP = a NDVI + b LST_{day} + c LST_{day} EVI + d	[-57.78 118 0.17 -0.33]	[23.79 48.54 0.08 0.16]	0.79	279	[-24.42 79.28 0.07 -0.21]	[9.19 36 0.03 0.12]	0.86	75	[231 -416.25 -0.83 1.51]	[105.9 145.1 0.37 0.50]	0.68	566	**[34.5 -119.1 -0.12 0.43]**	**[10.8 29.76 0.036 0.1]**	**0.60**	**34**	[0.43 -27.31 -0.01 0.14]	[3.17 7.05 0.01 0.024]	0.79	1226
GEP = a NDVI + b SW_{CERES} + c SW_{CERES} NDVI + d	[-9.6 23.6 0.02 -0.03]	[4.76 9.06 0.02 0.04]	0.79	277	[2.77 -11.51 -0.02 0.10]	[1.38 5.41 0.006 0.02]	0.87	62	**[13.58 -17.68 -0.12 0.198]**	**[6.53 8.95 0.032 0.04]**	**0.71**	**542**	**[2.74 -5.59 -0.02 0.07]**	**[0.88 2.32 0.005 0.014]**	**0.60**	**30**	**[-0.75 2.8 -0.01 0.05]**	**[0.37 0.75 0.001 0.003]**	**0.88**	**1013**
GEP = a SW_{CERES} + b SW_{CERES} NDVI + c	[2.63 -0.031 0.07]	[0.79 0.004 0.003]	0.78	277	[-0.15 -0.01 0.06]	[0.19 0.001 0.004]	0.88	64	**[0.72 -0.056 0.11]**	**[0.29 0.01 0.014]**	**0.71**	**542**	[0.69 -0.01 0.04]	[0.12 0.002 0.005]	0.57	30	[0.64 -0.016 0.058]	[0.12 0.0006 0.001]	0.87	1052

Table 3. Linear regressions obtained by a nonlinear mixed-effects regression model for Gross Ecosystem Productivity (GEP) versus combinations of 16-day average MODIS products: fixed solar zenith angle of 30˚ Enhanced Vegetation Index (EVI), daytime and Land Surface Temperature (LST_{day}), fixed solar zenith angle of 30˚ Normalized Difference Vegetation Index (NDVI), precipitation from the Tropical Rainfall Measuring Mission (TRMM) data product from 1998-2013 (NASA, 2014) (mm mo^{-1}), and surface shortwave incident radiation from the CERES (Kato et al., 2012). Model runs for HSP: Howard Springs, ASP: Alice Springs Mulga, CHO: Calperum-Chowilla, and TBR: Tumbarumba and all available data (includes all sites). EVI and NDVI labels are used instead of EVI_{SZA30} and $NDVI_{SZA30}$ for displaying purposes.